

# Effect of $\text{NO}_x$ level on secondary organic aerosol (SOA) formation from the photooxidation of terpenes

N. L. Ng<sup>1</sup>, P. S. Chhabra<sup>1</sup>, A. W. H. Chan<sup>1</sup>, J. D. Surratt<sup>2</sup>, J. H. Kroll<sup>3</sup>, A. J. Kwan<sup>4</sup>, D. C. McCabe<sup>4</sup>, P. O. Wennberg<sup>4</sup>, A. Sorooshian<sup>1</sup>, S. M. Murphy<sup>1</sup>, N. F. Dalleska<sup>4</sup>, R. C. Flagan<sup>1,4</sup>, and J. H. Seinfeld<sup>1,4</sup>

<sup>1</sup>Department of Chemical Engineering, California Institute of Technology, Pasadena, CA 91125, USA

<sup>2</sup>Department of Chemistry, California Institute of Technology, Pasadena, CA 91125, USA

<sup>3</sup>Aerodyne Research, Inc., Billerica, MA 01821, USA

<sup>4</sup>Department of Environmental Science and Engineering, California Institute of Technology, Pasadena, CA 91125, USA

Received: 7 June 2007 – Published in Atmos. Chem. Phys. Discuss.: 12 July 2007

Revised: 14 September 2007 – Accepted: 29 September 2007 – Published: 8 October 2007

**Abstract.** Secondary organic aerosol (SOA) formation from the photooxidation of one monoterpene ( $\alpha$ -pinene) and two sesquiterpenes (longifolene and aromadendrene) is investigated in the Caltech environmental chambers. The effect of  $\text{NO}_x$  on SOA formation for these biogenic hydrocarbons is evaluated by performing photooxidation experiments under varying  $\text{NO}_x$  conditions. The  $\text{NO}_x$  dependence of  $\alpha$ -pinene SOA formation follows the same trend as that observed previously for a number of SOA precursors, including isoprene, in which SOA yield (defined as the ratio of the mass of organic aerosol formed to the mass of parent hydrocarbon reacted) decreases as  $\text{NO}_x$  level increases. The  $\text{NO}_x$  dependence of SOA yield for the sesquiterpenes, longifolene and aromadendrene, however, differs from that determined for isoprene and  $\alpha$ -pinene; the aerosol yield under high- $\text{NO}_x$  conditions substantially exceeds that under low- $\text{NO}_x$  conditions. The reversal of the  $\text{NO}_x$  dependence of SOA formation for the sesquiterpenes is consistent with formation of relatively low-volatility organic nitrates, and/or the isomerization of large alkoxy radicals leading to less volatile products. Analysis of the aerosol chemical composition for longifolene confirms the presence of organic nitrates under high- $\text{NO}_x$  conditions. Consequently the formation of SOA from certain biogenic hydrocarbons such as sesquiterpenes (and possibly large anthropogenic hydrocarbons as well) may be more efficient in polluted air.

## 1 Introduction

Atmospheric oxidation of certain volatile organic compounds (VOCs) leads to the formation of low volatility species that partition into the condensed phase and form secondary organic aerosol (SOA). Biogenic hydrocarbons, such as isoprene ( $\text{C}_5\text{H}_8$ ), monoterpenes ( $\text{C}_{10}\text{H}_{16}$ ), and sesquiterpenes ( $\text{C}_{15}\text{H}_{24}$ ), are important contributors to the total atmospheric burden of SOA owing to their large global emissions and high reactivity with hydroxyl radicals (OH), ozone ( $\text{O}_3$ ), and nitrate radicals ( $\text{NO}_3$ ) (Guenther et al., 1995; Griffin et al., 1999a; Geron et al., 2000; Owen et al., 2001; Atkinson and Arey, 2003; Seinfeld and Pankow, 2003; Kanakidou et al., 2005).

Over the last two decades, numerous laboratory chamber experiments have been conducted to study aerosol formation from biogenic hydrocarbons. Level of odd nitrogen ( $\text{NO}_x$ ) has been found to be highly influential in SOA production for a variety of compounds. Recent studies on isoprene photooxidation,  $\alpha$ -pinene ozonolysis, and benzene, toluene, and *m*-xylene photooxidation have demonstrated that aerosol yields are generally highest at low levels of  $\text{NO}_x$  (Hatakeyama et al., 1991; Kroll et al., 2006; Presto et al., 2005; Song et al., 2005; Ng et al., 2007). These observations are consistent with competitive chemistry of peroxy radicals between NO and  $\text{HO}_2$ , with the  $\text{RO}_2+\text{HO}_2$  reaction producing products of lower volatility than the  $\text{RO}_2+\text{NO}$  reaction (Hatakeyama et al., 1991; Johnson et al., 2004, 2005; Kroll et al., 2005, 2006; Presto et al., 2005; Ng et al., 2007). For example, in  $\alpha$ -pinene ozonolysis, Presto et al. (2005) observed relatively volatile organic nitrates under high- $\text{NO}_x$  conditions, while less volatile products, such as 10-hydroxypinonic acid, were more abundant under low- $\text{NO}_x$  conditions. Although a

Correspondence to: J. H. Seinfeld  
(seinfeld@caltech.edu)

decreasing SOA yield with increasing NO<sub>x</sub> level has been established for relatively small hydrocarbons (10 carbons or fewer), it is unknown whether larger molecules, such as sesquiterpenes, exhibit a similar NO<sub>x</sub> dependence of SOA yield.

In the present study, we focus on two sesquiterpenes, longifolene and aromadendrene, and compare the NO<sub>x</sub>-dependence of their SOA formation with that of  $\alpha$ -pinene. Longifolene reacts very slowly with ozone (Atkinson and Arey, 2003), making it ideal for the study of OH photooxidation. Moreover, both longifolene and aromadendrene have only one double bond, thus one can infer more easily the general mechanisms of SOA formation than when multiple double bonds are present (Ng et al., 2006). Experiments are conducted under limiting NO<sub>x</sub> conditions (high-NO<sub>x</sub> conditions in which HONO is used as the OH precursor, and low-NO<sub>x</sub> conditions in which H<sub>2</sub>O<sub>2</sub> is used as the OH precursor), as well as with intermediate levels of NO<sub>x</sub>.

## 2 Experimental section

Experiments are performed in Caltech's dual 28 m<sup>3</sup> Teflon environmental chambers. Details of the facilities are given elsewhere (Cocker et al., 2001; Keywood et al., 2004). Before each experiment, the chambers are flushed continuously with dry purified air for  $\sim$ 24 h. Each chamber has a dedicated Differential Mobility Analyzer (DMA, TSI model 3081) coupled with a condensation nucleus counter (TSI model 3760) for measuring aerosol size distribution, number concentration, and volume concentration. All aerosol growth data are corrected for wall loss, in which size-dependent coefficients determined from inert particle wall loss experiments are applied to the aerosol volume data (Keywood et al., 2004). Temperature, relative humidity (RH), O<sub>3</sub>, NO, and NO<sub>x</sub> are continuously monitored. The initial temperature of the chamber is  $\sim$ 20°C. Heating from the lights leads to a temperature increase of approximately 5°C inside the chamber over the course of the experiment. The analytical instruments are located outside the chamber enclosure and are at the temperature of the surrounding room ( $\sim$ 20–22°C). The air may cool slightly as it is sampled from the chamber into the instruments, and the measured aerosol likely corresponds to the gas-particle partitioning at the temperature of the surrounding room rather than the chamber enclosure. Such small temperature differences are unlikely to affect results significantly.

Seed particles are introduced into the chamber to act as substrates onto which the gas-phase semivolatile products may condense. Seed aerosols are generated from a 0.015 M aqueous ammonium sulfate solution with a constant-rate atomizer, producing initial particle number concentrations of  $\sim$ 25 000 particles cm<sup>-3</sup>, with a geometric mean diameter of  $\sim$ 50 nm, and an initial aerosol seed volume of  $\sim$ 10–15  $\mu$ m<sup>3</sup> cm<sup>-3</sup>. After introduction of the seed aerosol, a

known volume of the parent hydrocarbon is injected into a glass bulb, and then introduced into the chambers by an air stream. For experiments with  $\alpha$ -pinene and longifolene, the concentration (mixing ratio) of the parent hydrocarbon is monitored with a Hewlett Packard gas chromatograph (model 5890) with flame ionization detection (GC-FID). The concentration of longifolene in several experiments is also measured with a Proton Transfer Reaction Mass Spectrometer (PTR-MS), a custom-modified Varian 1200 system (see Appendix A). Owing to the difficulties in measuring aromadendrene with GC-FID, its concentration is measured solely with the PTR-MS. The PTR-MS is calibrated only for aromadendrene.

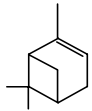
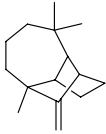
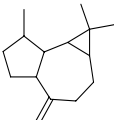
In the high-NO<sub>x</sub> experiments nitrous acid (HONO) serves as the OH precursor. HONO is prepared by dropwise addition of 15 mL of 1% NaNO<sub>2</sub> into 30 mL of 10% H<sub>2</sub>SO<sub>4</sub> in a glass bulb. After injection of the seed aerosol and parent hydrocarbon, the bulb is then attached to the chamber and a stream of dry air is passed through the bulb, sending HONO into the chamber. NO and NO<sub>2</sub>, formed as side products in the preparation of HONO, are also introduced into the chamber, and are measured by a commercial NO<sub>x</sub> monitor (Horiba APNA-360, Irvine, CA). Additional NO from a 500 ppm gas cylinder (Scott Marrin, Inc.) is introduced into the chamber after the addition of HONO to achieve a target NO<sub>x</sub> level in the chamber of about 1 ppm (upper limit of the NO<sub>x</sub> monitor).

For low-NO<sub>x</sub> experiments, H<sub>2</sub>O<sub>2</sub> serves as the OH precursor. The background NO<sub>x</sub> level in the chamber during such experiments is  $\leq$ 2 ppb. H<sub>2</sub>O<sub>2</sub> is introduced into the chamber (prior to introduction of seed particles and parent hydrocarbon) by bubbling air through a 50% H<sub>2</sub>O<sub>2</sub> solution for 2.5 h at 5 L/min. The concentration of H<sub>2</sub>O<sub>2</sub> in the chamber is not measured; based on the rate of hydrocarbon decay and literature values of  $\sigma_{\text{H}_2\text{O}_2}$  and  $k_{\text{H}_2\text{O}_2}$ , we estimate [H<sub>2</sub>O<sub>2</sub>] to be  $\sim$ 3–5 ppm (Kroll et al., 2006). The air stream then passes through a particle filter to remove any droplets. Variable NO experiments are also carried out, in which a known concentration of NO is introduced into the chamber after the addition of H<sub>2</sub>O<sub>2</sub>. This allows for the study of SOA formation under intermediate NO<sub>x</sub> conditions. It is noted that for these intermediate NO<sub>x</sub> experiments, NO goes to zero during the experiment and so there is a switch from high- to low-NO<sub>x</sub> conditions over the course of the experiment.

Once the seed, parent hydrocarbon, and NO<sub>x</sub> concentrations stabilize, reaction is initiated by irradiating the chamber with blacklights. Output from the lights is between 300 and 400 nm, with a maximum at 354 nm. Half of the available black lights are used in the experiments. At these wavelengths HONO efficiently photolyzes to OH and NO. By contrast, H<sub>2</sub>O<sub>2</sub> absorbs only weakly in this wavelength range, requiring the use of ppm mixing ratios of H<sub>2</sub>O<sub>2</sub> to achieve target levels of OH.

A comprehensive range of measurements are employed to study the chemical composition of the SOA formed.

**Table 1.** Parent hydrocarbons used in this study.

Parent Hydrocarbon	Structure	Formula (MW)	$k_{OH}$ (cm <sup>3</sup> molec <sup>-1</sup> s <sup>-1</sup> )
$\alpha$ -pinene		C <sub>10</sub> H <sub>16</sub> (136)	5.3 x 10 <sup>-11 a</sup>
longifolene		C <sub>15</sub> H <sub>24</sub> (204)	4.8 x 10 <sup>-11 a</sup>
aromadendrene		C <sub>15</sub> H <sub>24</sub> (204)	1.5 x 10 <sup>-10 b</sup>

<sup>a</sup> Rate constants were obtained from Atkinson et al. (2003).

<sup>b</sup> Rate constant was estimated from the rate of aromadendrene decay (experiment 1 in Table 4), assuming an OH concentration of 3 × 10<sup>6</sup> molecule cm<sup>-3</sup> and that aromadendrene reacts with OH only.

Real-time particle mass spectra are obtained with an Aerodyne quadrupole Aerosol Mass Spectrometer (Q-AMS) (Jayne et al., 2000). A particle-into-liquid sampler (PILS, Brechtel Manufacturing, Inc.) coupled with ion chromatography is employed for quantitative measurements of water-soluble ions in the aerosol phase (Sorooshian et al., 2006). For offline chemical analysis, aerosol samples are collected on Teflon filters (PALL Life Sciences, 47-mm diameter, 1.0- $\mu$ m pore size, Teflo membrane) starting at the point when aerosol volume reaches its maximum value. Depending on the total chamber volume concentration of aerosol, the filter sampling time is 2–4 h, which results in  $\sim$ 1.5–6 m<sup>3</sup> of total chamber air sampled. Teflon filter extraction protocols in HPLC-grade methanol have been described previously (Surratt et al., 2006). The resultant filter extracts are then analyzed by high performance liquid chromatography/electrospray ionization-quadrupole mass spectrometry (HPLC/ESI-MS) and electrospray ionization-ion trap mass spectrometry (ESI-ITMS); details of the protocols are described elsewhere (Surratt et al., 2006). Filter extracts are also analyzed by a Waters ACQUITY ultra performance liquid chromatography (UPLC) system, coupled with a Waters LCT Premier time-of-flight (TOF) mass spectrometer (MS) equipped with an electrospray ionization (ESI) source (see Appendix B), allowing for exact mass and tandem MS measurements.

The parent hydrocarbons studied and their stated purities are as follows:  $\alpha$ -pinene (Aldrich, 99+%), longifolene (Aldrich, >99%), and aromadendrene (Aldrich, >97%). Ta-

ble 1 lists the structures of the parent hydrocarbons and the rate constants of the compounds for reaction with OH radicals ( $k_{OH}$ ). Experimental conditions and results for each of the parent hydrocarbons studied are given in Tables 2, 3, and 4. In calculating SOA yield, knowledge of the SOA density is required. By comparing volume distributions from the DMA and mass distributions from the Q-AMS, effective densities for the SOA formed can be estimated (Baheini et al., 2005; Alfarra et al., 2006). The estimated densities of the SOA formed from different parent hydrocarbons are given in Table 5.

### 3 Aerosol yields

#### 3.1 $\alpha$ -pinene photooxidation

Under high-NO<sub>x</sub> conditions, the efficient photolysis of HONO generates relatively high concentrations of OH ( $\sim$ 2 × 10<sup>7</sup> molecules cm<sup>-3</sup> initially), leading to rapid  $\alpha$ -pinene decay. Aerosol growth occurs essentially immediately, even when [NO] is high (100's of ppb). With the high NO concentration throughout the entire experiment, formation of ozone and NO<sub>3</sub> is suppressed.

Under low-NO<sub>x</sub> conditions, aerosol growth is also observed immediately after initiation of irradiation. The  $\alpha$ -pinene decays at a slower rate than under high-NO<sub>x</sub> conditions, owing to the relatively slow production of OH radicals by H<sub>2</sub>O<sub>2</sub> photolysis. Ozone formation is observed at an increasing concentration over time ( $\sim$ 30 ppb at the peak

**Table 2.** Initial conditions and results for  $\alpha$ -pinene experiments.

Expt. No.	NO <sub>x</sub> Condition	NO (ppb)	NO <sub>2</sub> (ppb)	T (K)	RH (%)	$\Delta$ H C (ppb) <sup>a</sup>	$\Delta$ M <sub>0</sub> ( $\mu$ g/m <sup>3</sup> ) <sup>b</sup>	SOA Yield (%) <sup>c</sup>
1	H <sub>2</sub> O <sub>2</sub>	0	0	298	5.3	13.8±0.2	29.3±2.4	37.9±3.2
2	H <sub>2</sub> O <sub>2</sub>	0	1	298	6.2	47.5±0.8	121.3±9.4	45.8±3.6
3	H <sub>2</sub> O <sub>2</sub> +NO	198	0	296	6.4	13.1±0.2	15.6±1.4	21.2±2.0
4	HONO	475	463	299	3.3	12.6±0.2	4.5±0.9	6.6±1.4
5	HONO	390	578	298	3.7	46.6±0.8	40.8±3.8	15.8±1.5

<sup>a</sup> Stated uncertainties ( $1\sigma$ ) include scatter in GC measurements and GC calibration errors.

<sup>b</sup> Stated uncertainties ( $1\sigma$ ) are from scatter in particle volume measurements.

<sup>c</sup> Stated uncertainties are propagated from errors in  $\Delta$ H C and  $\Delta$ M<sub>0</sub>.

**Table 3.** Initial conditions and results for longifolene experiments.

Expt. No.	NO <sub>x</sub> Condition	NO (ppb)	NO <sub>2</sub> (ppb)	T (K)	RH (%)	$\Delta$ H C (ppb) <sup>b</sup>	$\Delta$ M <sub>0</sub> ( $\mu$ g/m <sup>3</sup> ) <sup>c</sup>	SOA Yield (%) <sup>d</sup>
1	H <sub>2</sub> O <sub>2</sub>	0	0	298	5.8	4.5±0.2	28.5±2.4	75.7±7.0
2	H <sub>2</sub> O <sub>2</sub>	0	2	297	6.0	8.4±0.4	52.5±4.2	74.4±6.7
3	H <sub>2</sub> O <sub>2</sub>	0	2	297	6.3	19.4±0.8	117.1±9.3	72.1±6.5
4	H <sub>2</sub> O <sub>2</sub>	0	2	299	5.7	24.8±1.1	148.4±11.6	71.8±6.4
5	H <sub>2</sub> O <sub>2</sub> +NO	70	31 <sup>a</sup>	297	6.2	3.8±0.2	35.8±2.9	111.7±10.2
6	H <sub>2</sub> O <sub>2</sub> +NO	209	26 <sup>a</sup>	297	8.0	4.7±0.2	43.4±3.5	110.2±10.0
7	H <sub>2</sub> O <sub>2</sub> +NO	316	0	298	6.4	4.1±0.2	43.4±3.5	127.2±1.5
8	H <sub>2</sub> O <sub>2</sub> +NO	394	0	297	6.1	4.8±0.2	50.0±4.1	124.9±11.5
9	H <sub>2</sub> O <sub>2</sub> +NO	564	0	297	6.2	3.9±0.2	51.6±4.1	157.0±14.1
10	HONO	428	550	298	3.7	9.7±0.4	68.3±5.1	84.0±7.1
11	HONO	469	502	298	3.7	19.6±0.9	141.9±10.3	86.8± 7.3
12	HONO	394	577	299	3.2	26.6±1.2	213.6±15.3	96.3±8.0

<sup>a</sup> NO<sub>2</sub> formed due to NO reacting with residual ozone in the chamber.

<sup>b</sup> Stated uncertainties ( $1\sigma$ ) include scatter in GC measurements and GC calibration errors.

<sup>c</sup> Stated uncertainties ( $1\sigma$ ) are from scatter in particle volume measurements.

<sup>d</sup> Stated uncertainties are propagated from errors in  $\Delta$ H C and  $\Delta$ M<sub>0</sub>.

of aerosol growth), possibly from residual material released from the chamber walls. Based on the reaction rate constants of  $\alpha$ -pinene+O<sub>3</sub> ( $k_{\text{ozone}}=8.4\times 10^{-17}$  cm<sup>3</sup> molecule<sup>-1</sup> s<sup>-1</sup>, Atkinson et al., 2003) and  $\alpha$ -pinene+OH ( $k_{\text{OH}}=5.3\times 10^{-11}$  cm<sup>3</sup> molecule<sup>-1</sup> s<sup>-1</sup>, Atkinson et al., 2003), and an inferred OH concentration of  $3\times 10^6$  molecules cm<sup>-3</sup> (estimated from longifolene low-NO<sub>x</sub> experiments, see Sect. 3.2), it is estimated that an ozone source of  $\sim 0.1$  ppb/min would be required to produce the observed  $\alpha$ -pinene decay. It is estimated that only about 35% of the  $\alpha$ -pinene reacts by ozonolysis at the point of maximum growth. Therefore, while  $\alpha$ -pinene ozonolysis accounts for some of the SOA yield under low-NO<sub>x</sub> conditions, it is unlikely that the observed yield differences between high- and low-NO<sub>x</sub> conditions (described below) arise solely from the presence of ozone.

Figure 1 shows the time-dependent growth curves (organic aerosol generated, denoted as  $\Delta$ M<sub>0</sub>, as a function of hydrocarbon reacted,  $\Delta$ H C) for  $\alpha$ -pinene under different NO<sub>x</sub> conditions. The curves are referred to as “time-dependent growth curves” as each curve represents aerosol growth data for a single experiment over the course of the experiment (Ng et al., 2006). As hydrocarbon measurements are made with a lower frequency than those of particle volume, the  $\alpha$ -pinene concentrations shown are obtained by fitting the GC measurements to an exponential decay. In all cases, the initial mixing ratio of  $\alpha$ -pinene is about 15 ppb, all of which is consumed by the end of the experiment. It is clear that the aerosol growth under low-NO<sub>x</sub> (H<sub>2</sub>O<sub>2</sub>) conditions substantially exceeds that under high-NO<sub>x</sub> (HONO) conditions, while the intermediate NO<sub>x</sub> (“H<sub>2</sub>O<sub>2</sub>+NO”) experiment exhibits an aerosol yield between those of the two extremes. The time-dependent growth curve of the intermediate NO<sub>x</sub>

**Table 4.** Initial conditions and results for aromadendrene experiments.

Expt. No.	NO <sub>x</sub> Condition	NO (ppb)	NO <sub>2</sub> (ppb)	T (K)	RH (%)	ΔHC (ppb) <sup>a</sup>	ΔM <sub>0</sub> (μg/m <sup>3</sup> ) <sup>b</sup>	SOA Yield (%)
1	H <sub>2</sub> O <sub>2</sub>	0	0	299	5.5	5.7±1.2	19.7±2.0	41.7±10
2	H <sub>2</sub> O <sub>2</sub> +NO	120	0	298	9.3	5.3±1.2	23.1±2.2	52.0±12.4
3	H <sub>2</sub> O <sub>2</sub> +NO	195	0	298	7.7	6.0±1.4	29.3±2.6	58.8±14.4
4	H <sub>2</sub> O <sub>2</sub> +NO	517	0	299	7.4	3.2±0.7	22.6±2.2	84.7±20.0

<sup>a</sup> Stated uncertainties (1σ) include scatter in PTR-MS measurements and PTR-MS calibration errors.

<sup>b</sup> Stated uncertainties are derived from scatter in particle volume measurements.

**Table 5.** Estimated effective SOA densities.

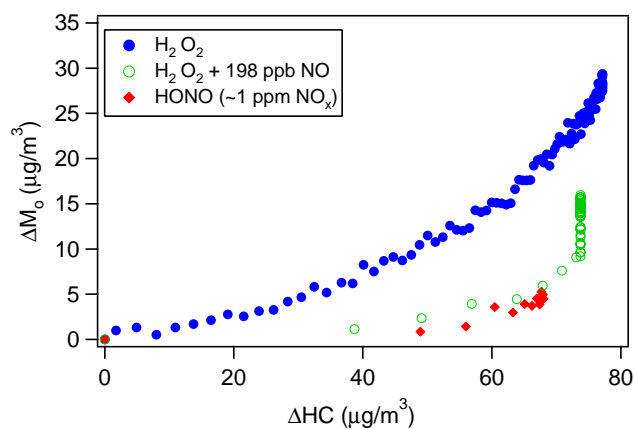
Parent Hydrocarbon	NO <sub>x</sub> Condition	Effective Density (g cm <sup>-3</sup> ) <sup>a</sup>
α-pinene	Low-NO <sub>x</sub>	1.32±0.10
α-pinene	Intermediate NO <sub>x</sub>	1.32±0.10
α-pinene	High-NO <sub>x</sub>	1.33±0.10
longifolene	Low-NO <sub>x</sub>	1.29±0.10
longifolene	Intermediate NO <sub>x</sub>	1.30±0.10
longifolene	High-NO <sub>x</sub>	1.40±0.10
aromadendrene	Low-NO <sub>x</sub>	1.20±0.10
aromadendrene	Intermediate NO <sub>x</sub>	1.35±0.10

<sup>a</sup> Stated uncertainties (1σ) are from repeated measurement of ammonium sulfate seed densities.

experiment exhibits a vertical section at the end, indicating that further reactions are contributing to aerosol growth after α-pinene is consumed. We return to this observation in Sect. 5.2.2.

### 3.2 Longifolene photooxidation

For longifolene, a series of high-NO<sub>x</sub> (HONO) experiments and low-NO<sub>x</sub> (H<sub>2</sub>O<sub>2</sub>) experiments with varying initial hydrocarbon concentrations are carried out. The time-dependent growth curves for 3 high-NO<sub>x</sub> and 3 low-NO<sub>x</sub> experiments, with initial longifolene mixing ratios ranging from ~10 to 30 ppb, are shown in Fig. 2. In contrast to α-pinene photooxidation, longifolene aerosol yields under high-NO<sub>x</sub> conditions exceed those under low-NO<sub>x</sub> conditions. Under high-NO<sub>x</sub> conditions, the maximum SOA yield is about ~100–130% and is reached in ~10 min after initiation of the experiments, with the yield decreasing after that point. It is noted that SOA yield is defined on a mass basis so oxidation (addition of O or N atoms) can lead to yields larger than 100%. Under low-NO<sub>x</sub> conditions, SOA yield continues to increase over the course of the experiment, reaching a maximum when all the longifolene is consumed. The final SOA yields of each longifolene low-NO<sub>x</sub> experiment lie on a straight line that passes through the origin, indicating that under low-NO<sub>x</sub> conditions SOA yield is constant (~75%) under the range of ΔM<sub>0</sub> studied. It is possible that under lower SOA loadings the yields

**Fig. 1.** Time-dependent growth curves for α-pinene photooxidation under different NO<sub>x</sub> conditions (Experiments 1, 3 and 4 in Table 2).

may decrease as some of the products partition back into the gas phase. Based on the observed longifolene decay and  $k_{OH}$  for longifolene, the chamber OH concentration under low-NO<sub>x</sub> conditions is estimated to be  $\sim 3 \times 10^6$  molecules cm<sup>-3</sup>.

The effect of NO<sub>x</sub> on longifolene aerosol formation is further illustrated by the time-dependent growth curves in Fig. 3. In both experiments H<sub>2</sub>O<sub>2</sub> is used as the OH precursor and the initial longifolene mixing ratio is 4–5 ppb; in one experiment no extra NO is added, while in the other experiment about 300 ppb of NO is introduced into the chamber after the addition of H<sub>2</sub>O<sub>2</sub>. Aerosol growth in the presence of ~300 ppb NO is substantially higher. A series of experiments with the same initial longifolene concentration but different initial NO concentrations (~100–600 ppb) are also carried out. Figure 4 shows the final aerosol yield as a function of the initial NO<sub>x</sub> concentration. The amount of aerosol formed is highly dependent on the level of NO<sub>x</sub> present initially; with ~600 ppb NO, the ultimate aerosol yield is twice that at low-NO<sub>x</sub> conditions.

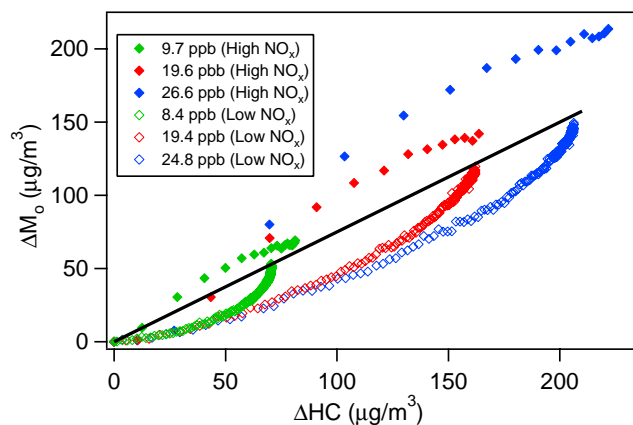


**Fig. 2.** Time-dependent growth curves for longifolene photooxidation under high- and low-NO<sub>x</sub> conditions (Experiments 2, 3, 4, 10, 11, and 12 in Table 3). The mixing ratios in the legend refer to the amount of longifolene reacted in each experiment. The final SOA yields of each low-NO<sub>x</sub> experiment lie on a straight line that passes through the origin, indicating that under low-NO<sub>x</sub> conditions SOA yield is constant, at ~75%.

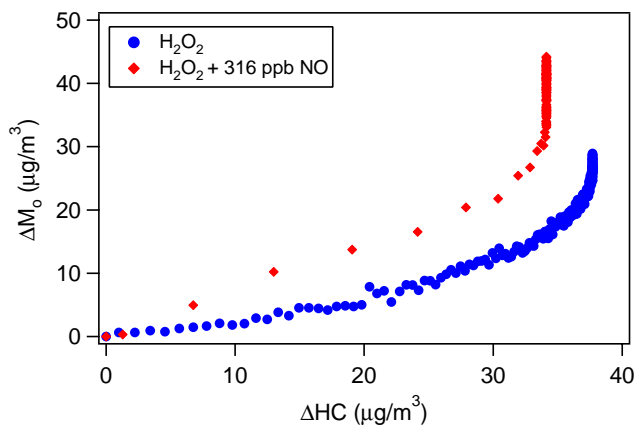


**Fig. 3.** Time-dependent growth curves for longifolene photooxidation with H<sub>2</sub>O<sub>2</sub> as the OH precursor. Aerosol growth in the presence of ~300 ppb NO (Experiment 7 in Table 3) significantly exceeds that without NO (Experiment 1 in Table 3).

### 3.3 Aromadendrene photooxidation

Figure 5 shows the final aerosol yield as a function of initial NO<sub>x</sub> concentration for aromadendrene photooxidation. The OH precursor used in these experiments is H<sub>2</sub>O<sub>2</sub> and the initial aromadendrene mixing ratio is ~5 ppb. It is clear that aromadendrene aerosol yield also increases with NO<sub>x</sub> concentration; as with longifolene, with ~500 ppb NO, the aerosol yield is approximately double that at low-NO<sub>x</sub> conditions.

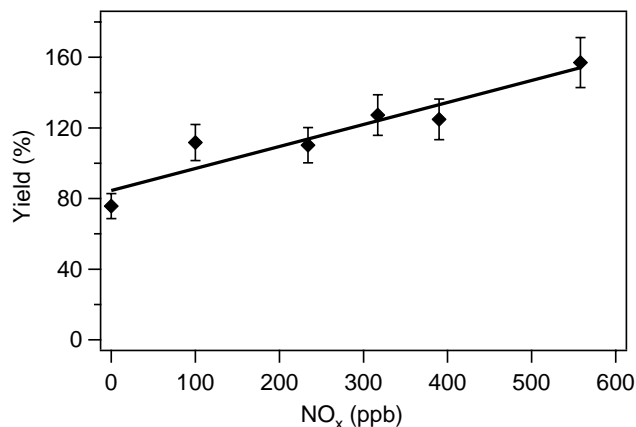


**Fig. 4.** SOA growth as a function of initial NO<sub>x</sub> concentration, for a fixed longifolene concentration (4–5 ppb). Results shown are from Table 3.

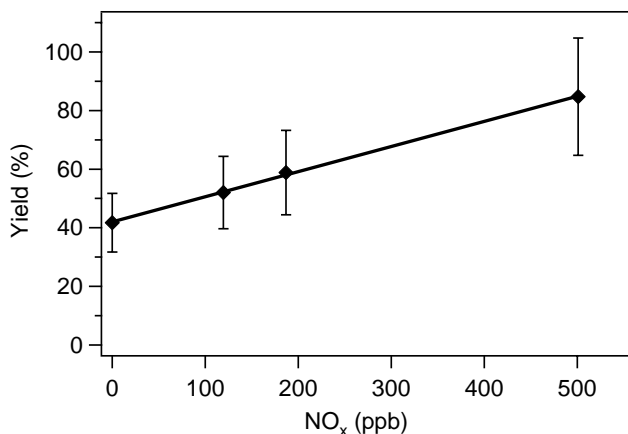


**Fig. 5.** SOA growth as a function of initial NO<sub>x</sub> concentration, at a fixed initial aromadendrene concentration (~5 ppb). Results shown are given in Table 4.

## 4 Chemical composition of SOA

In this section, the measurements of the chemical composition of  $\alpha$ -pinene and longifolene SOA are presented. The aromadendrene experiments are performed mainly to verify the observed NO<sub>x</sub> dependence for longifolene, in which SOA yield is higher under high-NO<sub>x</sub> conditions, and so detailed analysis of the chemical composition of aromadendrene SOA is not pursued.

### 4.1 Aerosol Mass Spectrometer (Q-AMS) measurements

Figures 6 and 7 show the AMS high-NO<sub>x</sub> versus low-NO<sub>x</sub> spectrum signal for  $\alpha$ -pinene and longifolene photooxidation, respectively. Each mass fragment is normalized by the total signal. For both hydrocarbons, SOA at high NO<sub>x</sub> conditions exhibit relatively strong signals at  $m/z$  30 and

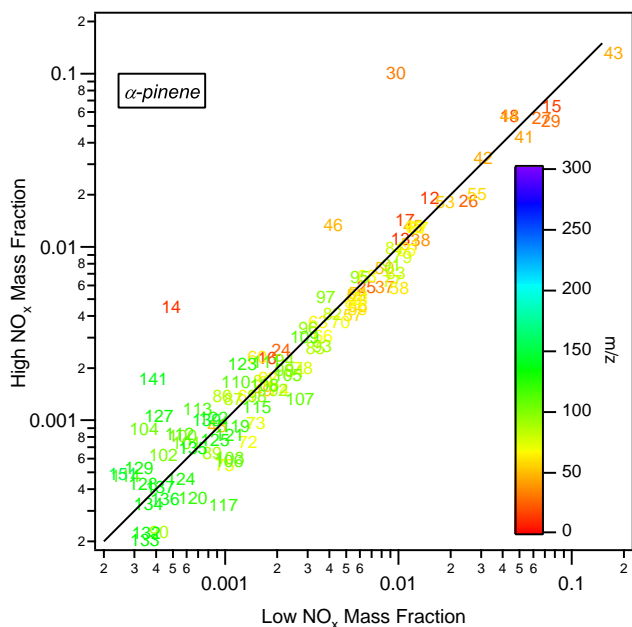


**Fig. 6.** AMS high-NO<sub>x</sub> spectra signal versus low-NO<sub>x</sub> spectra signal for  $\alpha$ -pinene photooxidation. Each mass fragment is normalized by the total signal. The solid black line is the 1:1 line. The spectra are taken when all hydrocarbon has been consumed.

46, and to a much smaller extent  $m/z$  14. The signals at these mass to charge ratios likely correspond to NO<sub>2</sub><sup>+</sup> (46), NO<sup>+</sup> (30), and N<sup>+</sup> (14) fragments from nitrates in the aerosol. The significance of these fragments will be further discussed in Sect. 5.1.

Changes in AMS spectra over the course of the experiment for longifolene under high- and low-NO<sub>x</sub> conditions are shown in Figs. 8 and 9, respectively. The corresponding growth curves for these experiments are shown in Fig. 2 (the pair of experiments with  $\sim 30$  ppb of longifolene injected). The top panel shows the fractional contribution of each mass fragment to the total organic and nitrate signal during the growth phase of the experiment (the first  $\sim 100 \mu\text{g m}^{-3}$  longifolene reacted); the middle panel shows the fractional contributions at the point when all of the hydrocarbon is consumed ( $\Delta\text{HC} \sim 200 \mu\text{g m}^{-3}$ ); the bottom panel shows the percentage change of each mass fragment between these two phases. Under high-NO<sub>x</sub> conditions, changes in mass fractions of different fragments during aerosol growth are minimal, indicating that the aerosol composition is not changing significantly over time. Under low-NO<sub>x</sub> conditions, however, the mass fraction of  $m/z$  44 (corresponding to the CO<sub>2</sub><sup>+</sup> ion, indicative of highly oxidized organics) increases by 93% during the reaction, while those for higher mass to charge ratios are observed to decrease. The mass fractions of  $m/z$  44 and higher mass to charge ratios continue to change even after the aerosol growth levels off, suggesting the presence of further chemistry (either gas-phase or particle-phase) even after all the initial hydrocarbon is consumed.

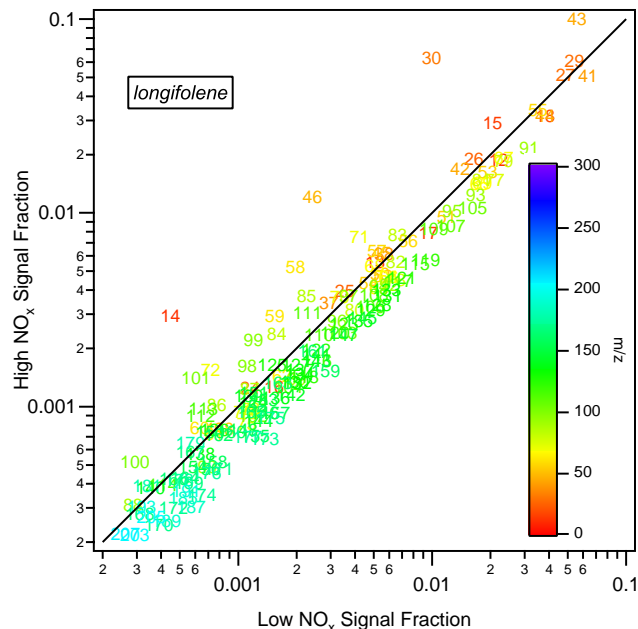


**Fig. 7.** AMS high-NO<sub>x</sub> spectra signal versus low-NO<sub>x</sub> spectra signal for longifolene photooxidation. Each mass fragment is normalized by the total signal. The solid black line is the 1:1 line. The spectra are taken when all hydrocarbon has been consumed.

#### 4.2 Offline chemical analysis

All ions detected by the UPLC/ESI-TOFMS instrument from  $\alpha$ -pinene and longifolene photooxidation are listed in Tables 6 and 7, respectively. The tables list the exact masses and their likely molecular formulas corresponding to each of the [M-H]<sup>-</sup> ions detected (in which M is the molecular weight of the compound). The error between the measured mass and theoretical mass is reported in two different ways, ppm and mDa. For most of the ions observed, the error between the measured and theoretical masses is less than  $\pm 2$  mDa and  $\pm 5$  ppm, allowing for generally unambiguous identification of molecular formulae. Solvent blanks and control filters are also run on the UPLC/ESI-TOFMS instrument; none of the listed ions is observed in these control samples. The ions listed in Tables 6 and 7 are also detected by HPLC/ESI-MS and ESI-ITMS, confirming that these compounds are not the result of artifact formation in a specific mass spectrometer.

Acidic compounds, such as carboxylic acids and sulfate esters, readily ionize under (-)ESI-MS techniques (Gao et al., 2004; Surratt et al., 2006; Surratt et al., 2007). Hydroxylated compounds, as well as ketones and aldehydes, however, are generally not ionizable unless carboxylic acid and/or sulfate ester moieties are also present within the same molecule. Therefore, it is expected that all ions listed in Tables 6 and 7 are acidic compounds. For the SOA formed in the presence of NO<sub>x</sub> (HONO and “H<sub>2</sub>O<sub>2</sub>+NO” experiments), even-mass

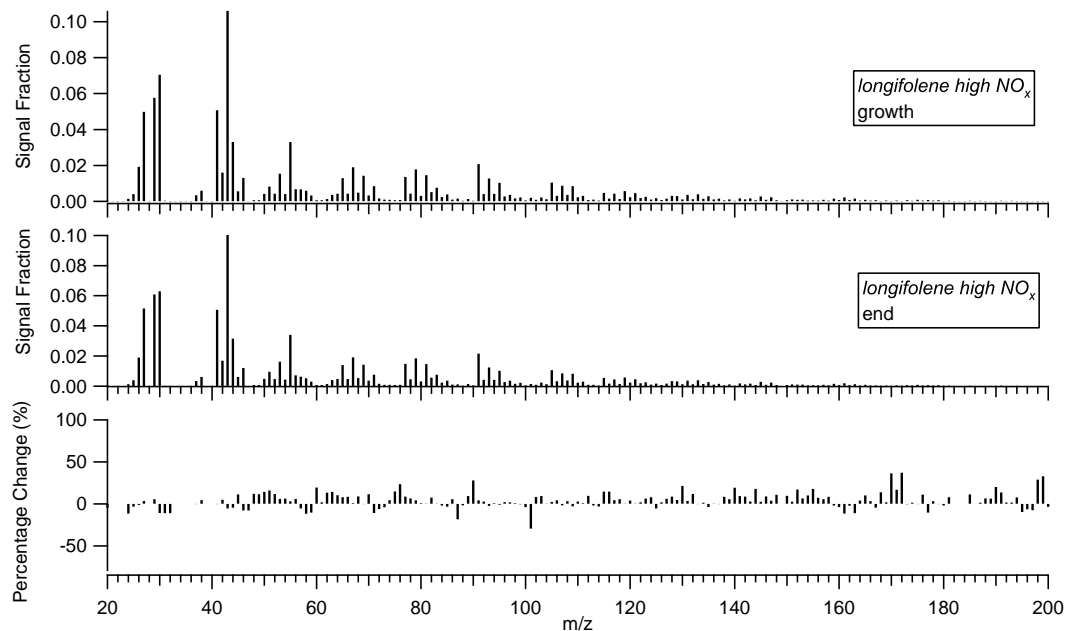


**Fig. 8.** Change in AMS spectrum over the course of longifolene photooxidation under high- $\text{NO}_x$  conditions. Top panel: Fractional contribution of each mass fragment to the total organic and nitrate signal during the growth phase of the experiment. Middle panel: fractional contribution of each mass fragment to the total organic and nitrate signal when all hydrocarbon is consumed. Bottom panel: Percentage change of each mass fragment between the growth phase and the end of the experiment.

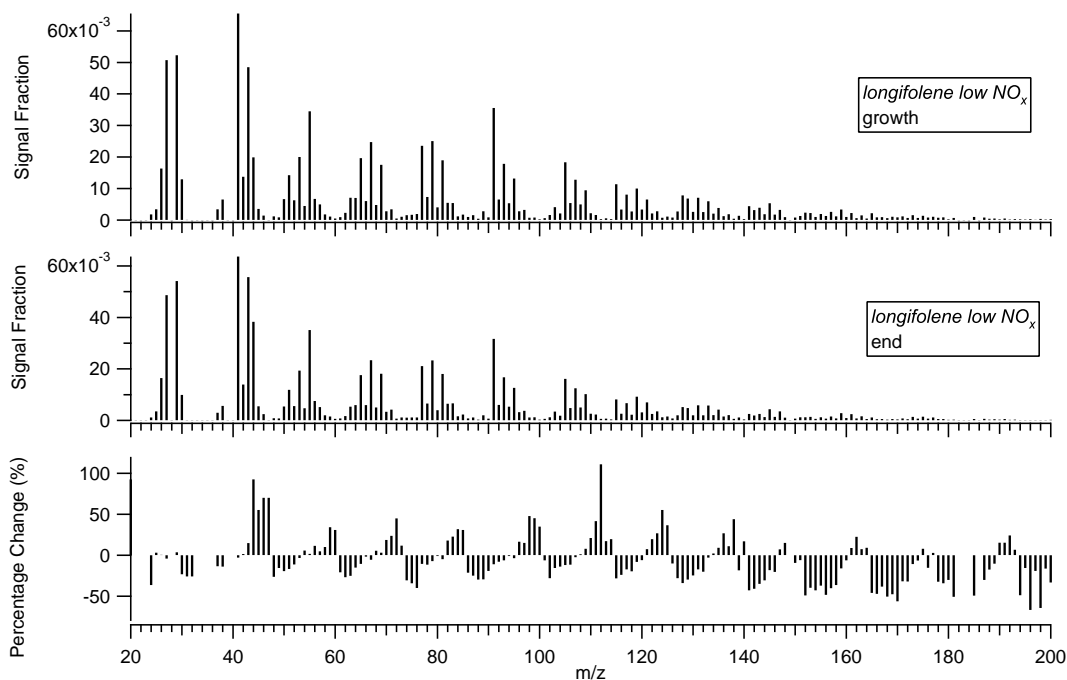


**Fig. 9.** Change in AMS spectrum over the course of longifolene photooxidation under low- $\text{NO}_x$  conditions. Top panel: Fractional contribution of each mass fragment to the total organic and nitrate signal during the growth phase of the experiment. Middle panel: fractional contribution of each mass fragment to the total organic and nitrate signal when all hydrocarbon is consumed. Bottom panel: Percentage change of each mass fragment between the growth phase and the end of the experiment.



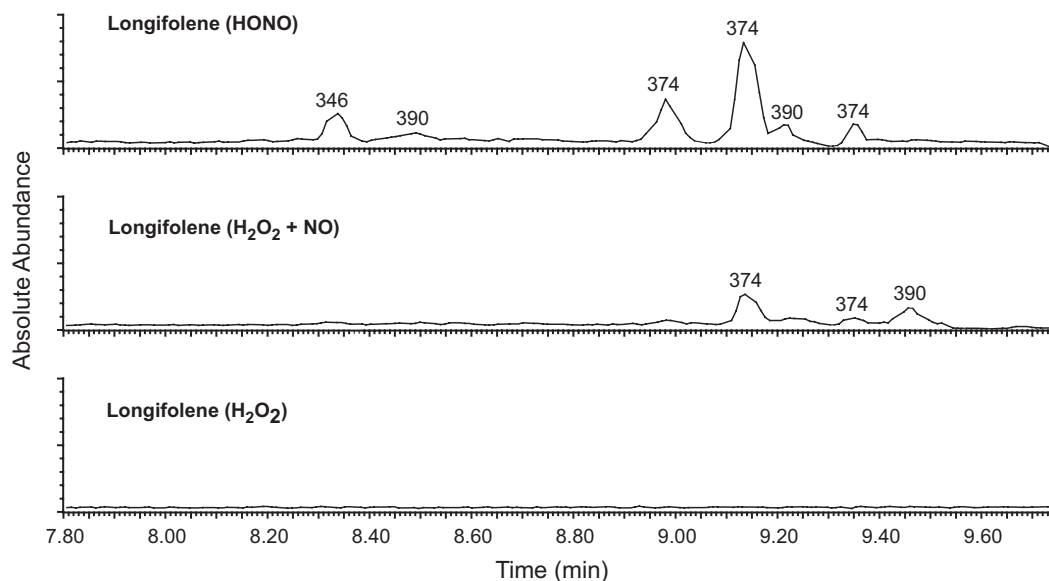


**Fig. 10.** UPLC/ESI-TOFMS extracted ion chromatograms (EICs) ( $m/z$  346+374+390) for longifolene photooxidation. The even  $[M-H]^-$  ions listed above the chromatographic peaks correspond to organic nitrates detected in longifolene SOA. No organic nitrates are detected in the H<sub>2</sub>O<sub>2</sub> experiment (low-NO<sub>x</sub> condition). The HONO experiment (high-NO<sub>x</sub> condition) has the widest array of organic nitrates detected (as shown in Table 7), as well as the largest chromatographic peaks;  $m/z$  372 is the only exception, and is most abundant in the intermediate NO<sub>x</sub> experiment. These EICs are directly comparable as the volume of chamber air sampled is approximately the same (2 m<sup>3</sup>).

$[M-H]^-$  ions are observed in ESI mass spectra, indicating the compound has an odd number of nitrogen atoms, likely within organic nitrate functional groups. Nitrated organics were previously observed in isoprene SOA formed under high-NO<sub>x</sub> conditions (both HONO and H<sub>2</sub>O<sub>2</sub>+NO) (Surratt et al., 2006), and are further confirmed by the tandem MS data, which reveals a loss of 63 Da (HNO<sub>3</sub>). For  $\alpha$ -pinene, only one acidic organic nitrate ( $m/z$  322) is detected in the HONO experiment and none are detected in H<sub>2</sub>O<sub>2</sub> and intermediate NO<sub>x</sub> experiments. Masses of many ions detected in the  $\alpha$ -pinene experiments have been observed in previous laboratory work (Glasius et al., 1999, 2000; Larsen et al., 2001) and field studies (Gao et al., 2006). For longifolene, a much wider array of acidic organic nitrates is detected by the UPLC/ESI-TOFMS instrument in both HONO and intermediate NO<sub>x</sub> experiments. For both  $\alpha$ -pinene and longifolene, compounds with more carbons than the parent hydrocarbon are observed. Tandem MS data for these C<sub>12</sub>, C<sub>16</sub>, and C<sub>17</sub> acidic organic nitrates reveal a common neutral loss of 60 Da, which possibly corresponds to an acetic acid monomer. Surratt et al. (2006) and Szmigielski et al. (2007) recently showed that particle-phase esterification occurs in isoprene SOA formed under high-NO<sub>x</sub> conditions. The observed neutral loss of 60 Da for these acidic organic nitrates suggests that these compounds may be dimers formed by particle-phase esterification.

Figure 10 shows the extracted ion chromatograms (EICs) of  $m/z$  346, 374, and 390 from longifolene oxidation under different NO<sub>x</sub> conditions. These  $m/z$  values correspond to

acidic organic nitrates, as confirmed by the exact mass data (Table 7) as well as the loss of 63 Da in the tandem MS data. The chromatographic peaks are much larger in the highest NO<sub>x</sub> experiment than those in the intermediate NO<sub>x</sub> experiment (except  $m/z$  372, not shown); no chromatographic peaks are observed under low-NO<sub>x</sub> (H<sub>2</sub>O<sub>2</sub>) conditions. In addition, for several  $[M-H]^-$  ions (e.g.  $m/z$  374 and 390) there are several structural isomers present. Additionally, the intensity of non-nitrogen-containing ions (e.g.  $m/z$  223, 239, 253, 255, 267, 269, and 283), are generally larger under low-NO<sub>x</sub> conditions.

## 5 Discussion

### 5.1 Effect of hydrocarbon size on NO<sub>x</sub> dependence

It has been established that NO<sub>x</sub> levels exert a major influence on SOA formation (Hatakeyama et al., 1991; Pandis et al., 1991; Zhang et al., 1992, 2006; Hurley et al., 2001; Johnson et al., 2004, 2005; Song et al., 2005; Presto et al., 2005; Kroll et al., 2005, 2006; Ng et al., 2007). For photooxidation of isoprene, SOA yields increase as the NO<sub>x</sub> level decreases (Kroll et al., 2006). The proposed mechanism for this observed NO<sub>x</sub> dependence is the competitive chemistry of organic peroxy radicals between NO and HO<sub>2</sub>, in which the semivolatile products formed via the RO<sub>2</sub>+HO<sub>2</sub> path are less volatile than those formed via the RO<sub>2</sub>+NO route (Hatakeyama et al., 1991; Johnson et al., 2004, 2005;

**Table 6.**  $\alpha$ -Pinene acidic SOA components detected by UPLC/ESI-TOFMS.

Experiment	Measured [M - H] <sup>-</sup> ion ( <i>m/z</i> )	TOFMS suggested molecular formula	Error (mDa)	Error (ppm)	Retention Time (min)
H <sub>2</sub> O <sub>2</sub>	157.0497	C <sub>7</sub> H <sub>9</sub> O <sub>4</sub> <sup>-</sup>	-0.4	-2.5	5.09
	169.0873	C <sub>9</sub> H <sub>13</sub> O <sub>3</sub> <sup>-</sup>	0.8	4.7	6.89
	171.0654	C <sub>8</sub> H <sub>11</sub> O <sub>4</sub> <sup>-</sup>	-0.3	-1.8	5.61
	183.1027	C <sub>10</sub> H <sub>15</sub> O <sub>3</sub> <sup>-</sup>	0.6	3.3	7.50
	185.0821	C <sub>9</sub> H <sub>13</sub> O <sub>4</sub> <sup>-</sup>	0.7	3.8	6.85
	199.0983	C <sub>10</sub> H <sub>15</sub> O <sub>4</sub> <sup>-</sup>	1.3	6.5	6.17
	199.0982	C <sub>10</sub> H <sub>15</sub> O <sub>4</sub> <sup>-</sup>	1.2	6.0	6.29
	199.0976	C <sub>10</sub> H <sub>15</sub> O <sub>4</sub> <sup>-</sup>	0.6	3.0	6.34
	215.0923	C <sub>10</sub> H <sub>15</sub> O <sub>5</sub> <sup>-</sup>	0.4	1.9	5.99
	215.0930	C <sub>10</sub> H <sub>15</sub> O <sub>5</sub> <sup>-</sup>	1.1	5.1	7.18
231.0885	C <sub>10</sub> H <sub>15</sub> O <sub>6</sub> <sup>-</sup>	1.6	6.9	6.80	
H <sub>2</sub> O <sub>2</sub> + NO	157.0499	C <sub>7</sub> H <sub>9</sub> O <sub>4</sub> <sup>-</sup>	-0.2	-1.3	5.08
	171.0655	C <sub>8</sub> H <sub>11</sub> O <sub>4</sub> <sup>-</sup>	-0.2	-1.2	5.60
	183.1025	C <sub>10</sub> H <sub>15</sub> O <sub>3</sub> <sup>-</sup>	0.4	2.2	7.49
	185.0812	C <sub>9</sub> H <sub>13</sub> O <sub>4</sub> <sup>-</sup>	-0.2	-1.1	6.86
	197.0814	C <sub>10</sub> H <sub>15</sub> O <sub>4</sub> <sup>-</sup>	0.0	0.0	8.09
	199.0971	C <sub>10</sub> H <sub>15</sub> O <sub>4</sub> <sup>-</sup>	0.1	0.5	6.36
	203.0557	C <sub>8</sub> H <sub>11</sub> O <sub>6</sub> <sup>-</sup>	0.1	0.5	5.50
	215.0925	C <sub>10</sub> H <sub>15</sub> O <sub>5</sub> <sup>-</sup>	0.6	2.8	6.23
	229.0718	C <sub>10</sub> H <sub>13</sub> O <sub>6</sub> <sup>-</sup>	0.6	2.6	6.17
	231.0856	C <sub>10</sub> H <sub>15</sub> O <sub>6</sub> <sup>-</sup>	-1.3	-5.6	6.79
HONO	171.0649	C <sub>8</sub> H <sub>11</sub> O <sub>4</sub> <sup>-</sup>	-0.8	-4.7	5.60
	183.1022	C <sub>10</sub> H <sub>15</sub> O <sub>3</sub> <sup>-</sup>	0.1	0.5	7.49
	185.0457	C <sub>8</sub> H <sub>9</sub> O <sub>5</sub> <sup>-</sup>	0.7	3.8	6.63
	187.0606	C <sub>8</sub> H <sub>11</sub> O <sub>5</sub> <sup>-</sup>	0.0	0.0	5.65
	197.0819	C <sub>10</sub> H <sub>13</sub> O <sub>4</sub> <sup>-</sup>	0.5	2.5	8.09
	203.0546	C <sub>8</sub> H <sub>11</sub> O <sub>6</sub> <sup>-</sup>	-1.0	-4.9	5.50
	213.0781	C <sub>10</sub> H <sub>13</sub> O <sub>5</sub> <sup>-</sup>	1.8	8.4	5.26
	231.0883	C <sub>10</sub> H <sub>15</sub> O <sub>6</sub> <sup>-</sup>	1.4	6.1	6.80
	259.1182	C <sub>12</sub> H <sub>19</sub> O <sub>6</sub> <sup>-</sup>	0.0	0.0	5.85
	322.1148	C <sub>12</sub> H <sub>20</sub> NO <sub>9</sub> <sup>-</sup>	1.0	3.1	7.62

Presto et al., 2005; Kroll et al., 2006; Zhang et al., 2006; Ng et al., 2007). A similar yield dependence on NO<sub>x</sub> is observed here for photooxidation of  $\alpha$ -pinene (Fig. 1). For an initial  $\alpha$ -pinene concentration of  $\sim 15$  ppb, the SOA yield under low-NO<sub>x</sub> conditions is about a factor of 3 higher than that under high-NO<sub>x</sub> conditions. The observed NO<sub>x</sub> dependence is consistent with that of previous studies on  $\alpha$ -pinene photooxidation (Hatakeyama et al., 1991) and  $\alpha$ -pinene ozonolysis (Presto et al., 2005).

The observed NO<sub>x</sub> dependence of SOA yield for the sesquiterpenes, however, is different from that of isoprene and  $\alpha$ -pinene (as well as other hydrocarbons with 10 or fewer carbons, such as aromatic species). For longifolene and aromadendrene, aerosol yield increases with increasing NO<sub>x</sub> concentration (Figs. 2–5). This reversal of the NO<sub>x</sub> dependence of SOA formation could be the result of a number of factors. Figure 11 shows a simplified reaction mechanism involving peroxy radical chemistry. At the two limiting NO<sub>x</sub> conditions of this study, the peroxy radical chemistry is relatively well-defined; under high-NO<sub>x</sub> conditions, peroxy radicals react virtually entirely with NO, while under low-NO<sub>x</sub> conditions, RO<sub>2</sub> reacts predominantly with HO<sub>2</sub>. One of the possible explanations for the higher SOA yield under high-NO<sub>x</sub> conditions is the formation of large alkoxy radicals that isomerize rather than fragment. Isomerization is plausible if

**Table 7.** Longifolene acidic SOA components detected by UPLC/ESI-TOFMS.

Experiment	Measured [M - H] <sup>-</sup> ion ( <i>m/z</i> )	TOFMS suggested molecular formula	Error (mDa)	Error (ppm)	Retention Time (min)
H <sub>2</sub> O <sub>2</sub>	223.1344	C <sub>13</sub> H <sub>19</sub> O <sub>3</sub> <sup>-</sup>	1.0	4.5	8.92
	237.1500	C <sub>14</sub> H <sub>21</sub> O <sub>3</sub> <sup>-</sup>	0.9	3.8	9.06
	239.1651	C <sub>14</sub> H <sub>23</sub> O <sub>3</sub> <sup>-</sup>	0.4	1.7	10.50
	253.1445	C <sub>14</sub> H <sub>21</sub> O <sub>4</sub> <sup>-</sup>	0.5	2.0	9.36
	249.1499	C <sub>15</sub> H <sub>21</sub> O <sub>4</sub> <sup>-</sup>	0.8	3.2	9.25
	249.1501	C <sub>15</sub> H <sub>21</sub> O <sub>4</sub> <sup>-</sup>	1.0	4.0	10.14
	255.1611	C <sub>14</sub> H <sub>23</sub> O <sub>4</sub> <sup>-</sup>	1.5	5.9	9.88
	255.1622	C <sub>14</sub> H <sub>23</sub> O <sub>4</sub> <sup>-</sup>	2.6	10.2	8.99
	267.1602	C <sub>15</sub> H <sub>23</sub> O <sub>4</sub> <sup>-</sup>	0.6	2.2	8.88
	267.1606	C <sub>15</sub> H <sub>23</sub> O <sub>4</sub> <sup>-</sup>	1.0	3.7	9.01
	267.1611	C <sub>15</sub> H <sub>23</sub> O <sub>4</sub> <sup>-</sup>	1.5	5.6	9.28
	267.1601	C <sub>15</sub> H <sub>23</sub> O <sub>4</sub> <sup>-</sup>	0.5	1.9	9.70
	269.1392	C <sub>14</sub> H <sub>21</sub> O <sub>5</sub> <sup>-</sup>	0.3	1.1	7.71
	283.1561	C <sub>15</sub> H <sub>23</sub> O <sub>5</sub> <sup>-</sup>	1.6	5.7	7.35
	313.2018	C <sub>17</sub> H <sub>29</sub> O <sub>5</sub> <sup>-</sup>	0.3	1.0	9.20
H <sub>2</sub> O <sub>2</sub> + NO	223.1337	C <sub>13</sub> H <sub>19</sub> O <sub>3</sub> <sup>-</sup>	0.3	1.3	8.92
	239.1649	C <sub>14</sub> H <sub>23</sub> O <sub>3</sub> <sup>-</sup>	0.2	0.8	10.49
	265.1442	C <sub>15</sub> H <sub>21</sub> O <sub>4</sub> <sup>-</sup>	0.2	0.8	8.93
	269.1401	C <sub>14</sub> H <sub>21</sub> O <sub>5</sub> <sup>-</sup>	1.2	4.5	7.72
	316.1396	C <sub>14</sub> H <sub>22</sub> NO <sub>7</sub> <sup>-</sup>	0.0	0.0	9.88
	329.1972	C <sub>17</sub> H <sub>29</sub> O <sub>6</sub> <sup>-</sup>	0.8	2.4	9.35
	372.1664	C <sub>17</sub> H <sub>26</sub> NO <sub>8</sub> <sup>-</sup>	0.6	1.6	10.58
	374.1829	C <sub>17</sub> H <sub>28</sub> NO <sub>8</sub> <sup>-</sup>	1.4	3.7	9.14
	374.1829	C <sub>17</sub> H <sub>28</sub> NO <sub>8</sub> <sup>-</sup>	1.4	3.7	9.35
	390.1775	C <sub>17</sub> H <sub>28</sub> NO <sub>9</sub> <sup>-</sup>	1.1	2.8	9.46
	223.1334	C <sub>13</sub> H <sub>19</sub> O <sub>3</sub> <sup>-</sup>	-0.1	-0.4	8.92
	241.1453	C <sub>13</sub> H <sub>21</sub> O <sub>4</sub> <sup>-</sup>	1.3	5.4	7.55
	253.1431	C <sub>14</sub> H <sub>21</sub> O <sub>4</sub> <sup>-</sup>	-0.9	-3.6	8.02
	269.1394	C <sub>14</sub> H <sub>21</sub> O <sub>5</sub> <sup>-</sup>	0.5	1.9	7.18
	269.1408	C <sub>14</sub> H <sub>21</sub> O <sub>5</sub> <sup>-</sup>	1.9	7.1	7.71
342.1930	C <sub>17</sub> H <sub>28</sub> NO <sub>6</sub> <sup>-</sup>	1.3	3.8	9.65	
344.1348	C <sub>15</sub> H <sub>22</sub> NO <sub>8</sub> <sup>-</sup>	0.3	0.9	8.25	
346.1502	C <sub>15</sub> H <sub>24</sub> NO <sub>8</sub> <sup>-</sup>	0.2	0.6	8.34	
360.1674	C <sub>16</sub> H <sub>26</sub> NO <sub>8</sub> <sup>-</sup>	1.6	4.4	8.89	
372.1667	C <sub>17</sub> H <sub>26</sub> NO <sub>8</sub> <sup>-</sup>	-0.6	-1.6	10.61	
374.1809	C <sub>17</sub> H <sub>28</sub> NO <sub>8</sub> <sup>-</sup>	-0.6	-1.6	8.89	
374.1816	C <sub>17</sub> H <sub>28</sub> NO <sub>8</sub> <sup>-</sup>	0.1	0.3	9.13	
374.1808	C <sub>17</sub> H <sub>28</sub> NO <sub>8</sub> <sup>-</sup>	-0.7	-1.9	9.35	
390.1773	C <sub>17</sub> H <sub>28</sub> NO <sub>9</sub> <sup>-</sup>	0.9	2.3	8.49	
390.1778	C <sub>17</sub> H <sub>28</sub> NO <sub>9</sub> <sup>-</sup>	1.4	3.6	9.21	
435.1619	C <sub>17</sub> H <sub>27</sub> N <sub>2</sub> O <sub>11</sub> <sup>-</sup>	0.4	0.9	9.56	

the alkoxy radical has four or more carbon atoms and can form a 6-membered transition state (Baldwin et al., 1977; Carter and Atkinson, 1985). The isomerization pathway leads to the formation of large hydroxycarbonyls, multifunctional products that are likely low in volatility. The relative importance of isomerization increases with the size of alkoxy radicals (Atkinson, 1994, 1997a, b; Atkinson et al., 1995, 1999), and larger compounds could exhibit increasing SOA yields under high-NO<sub>x</sub> conditions as a consequence of this mechanism. For example, Lim and Ziemann (2005) measured SOA yields up to  $\sim 50\%$  for C<sub>15</sub> alkanes in the presence of ppm levels of NO<sub>x</sub>. They proposed multiple isomerization steps leading to the formation of multifunctional compounds including nitrooxy, hydroxyl, and carbonyl groups, and it is suggested that the hydroxycarbonyls formed may isomerize to form furan species that can undergo further reactions (Lim and Ziemann, 2005). Gas-phase products that are consistent with the isomerization mechanism have been observed

in  $\alpha$ -pinene photooxidation but this pathway does not appear to dominate SOA formation under high-NO<sub>x</sub> conditions (Aschmann et al., 1998, 2002), possibly due to the higher volatility of these species.

Higher SOA yields observed under high-NO<sub>x</sub> conditions for sesquiterpenes may, secondly, be a result of the formation of relatively nonvolatile organic nitrates, evidence for which appears in both Q-AMS data and filter sample data. In AMS data,  $m/z$  30 (NO<sup>+</sup>) and  $m/z$  46 (NO<sub>2</sub><sup>+</sup>) signals are commonly associated with nitrate species (organic and inorganic nitrates). For both  $\alpha$ -pinene and longifolene, the ratio of the sum of the intensities of ions at  $m/z$  30 and  $m/z$  46 to the total ion intensity is higher under high-NO<sub>x</sub> conditions: under low-NO<sub>x</sub> conditions, the ratio is very small (2%), under high-NO<sub>x</sub> conditions, the ratio is about 15–25%. The ratio of  $m/z$  30 to total mass and the ratio of  $m/z$  46 to total mass show the same trend, indicating  $m/z$  30 and  $m/z$  46 are correlated. It is possible that the signal at  $m/z$  30 could be the result of a non-nitrogen containing organic fragment ion; however, given the observed correlation between  $m/z$  30 and  $m/z$  46 and their small signals under low-NO<sub>x</sub> conditions, it appears that there is little interference from organics at these signals. Under high-NO<sub>x</sub> conditions,  $\sim 10 \mu\text{g m}^{-3}$  of inorganic nitrates, as measured by the PILS/IC, are present in the aerosol. Such nitrates may arise from the partitioning or reactive uptake of gas-phase HNO<sub>3</sub> into the aerosol phase. Assuming no non-nitrate contribution to  $m/z$  30 and  $m/z$  46, the total nitrate content of the SOA is estimated as the sum of the signals at each fragment. It is found that the calculated nitrate content ( $\sim 20 \mu\text{g m}^{-3}$ ) exceeds that measured by PILS/IC, suggesting the presence of organic nitrates.

The filter sample data provide a more direct comparison on the amount of organic nitrates formed in  $\alpha$ -pinene and longifolene photooxidation under different NO<sub>x</sub> conditions. For both  $\alpha$ -pinene and longifolene, no acidic nitrates are observed under low-NO<sub>x</sub> conditions, consistent with the lack of NO<sub>x</sub> and the prevailing RO<sub>2</sub>+HO<sub>2</sub> reaction in this case. Organic nitrate yield from the RO<sub>2</sub>+NO reaction increases with increasing carbon number (Atkinson et al., 1987; Carter and Atkinson, 1989; O'Brien et al., 1998; Arey et al., 2001; Aschmann et al., 2001; Zhang et al., 2004), and with the larger carbon skeleton the organic nitrates formed will be less volatile, this is consistent with the much wider array and larger quantities of acidic nitrates detected in longifolene photooxidation under high-NO<sub>x</sub> conditions compared to the  $\alpha$ -pinene experiments. Hence for photooxidation of larger compounds such as sesquiterpenes, the nitrate formation channel may play an important role in SOA formation under high-NO<sub>x</sub> conditions. With the formation of large molecular weight compounds with nitrate groups, mass-based SOA yields from longifolene photooxidation under high-NO<sub>x</sub> conditions actually exceed 100%.

Lacking appropriate analytical techniques for the detection of non-acidic nitrates, the contribution of these species under high-NO<sub>x</sub> conditions cannot be assessed. In  $\alpha$ -pinene

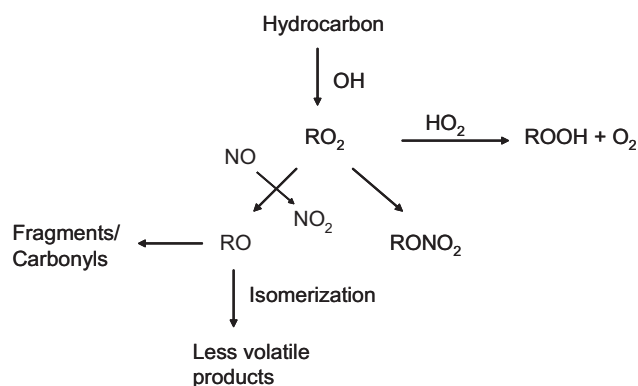


**Fig. 11.** General schematic of gas-phase peroxy radical chemistry in SOA formation.

photooxidation, hydroxynitrates have been identified in the gas phase using mass spectrometry (Aschmann et al., 1998, 2002). In SOA formation from alkanes under high-NO<sub>x</sub> conditions, Lim and Ziemann (2005) found that, while SOA from oxidation of C<sub>10</sub> alkane contains no  $\delta$ -hydroxynitrates, nitrates contribute  $\sim 40\%$  of the SOA mass for reactions of the C<sub>15</sub> alkane. It seems likely that higher levels of hydroxynitrates are present in longifolene SOA than in  $\alpha$ -pinene SOA.

## 5.2 General mechanisms of aerosol growth

### 5.2.1 Loss of semivolatiles

Substantial insight into the general mechanism of SOA formation and growth kinetics can be gained by examining “growth curves”, showing the amount of SOA formed per hydrocarbon reacted (Ng et al., 2006, 2007). Figure 2 shows the time-dependent growth curves from longifolene photooxidation under high- and low-NO<sub>x</sub> conditions. The high-NO<sub>x</sub> growth curves have a “convex” shape, indicating that aerosol growth slows down as longifolene approaches complete reaction. Similar behavior for longifolene growth was observed previously in our laboratory (Ng et al., 2006); the authors suggested that this atypical growth behavior may have been spurious, as a result of inaccuracies in PTR-MS measurements, owing to interference from product ions, or changes in the aerosol density over the course of the experiment. In this study, in those experiments in which the longifolene concentration is monitored by both GC-FID and PTR-MS, the shape of PTR-MS hydrocarbon decay agrees with that measured by GC-FID. The density of the aerosol is estimated during oxidation by comparing Q-AMS and DMA data. It is found that the SOA density decreases slightly ( $< 5\%$ ) over the course of the experiment, however, such a small decrease in density is within experimental uncertainty and cannot account for the observed atypical growth behavior.

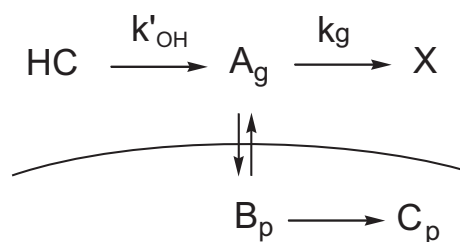


**Fig. 12.** A kinetic scheme depicting the competition between gas-particle partitioning and irreversible loss of the gas-phase semivolatiles. X represents the product of generic loss of semivolatile species  $A_g$  by chemical reaction, and/or loss to chamber walls.  $k'_{\text{OH}}$  is the pseudo-first-order rate constant ( $k'_{\text{OH}}=k_{\text{OH}}[\text{OH}]$ ) for photooxidation of the parent hydrocarbon;  $k_g$  is the first-order rate constant of loss of semivolatiles.

Deceleration in SOA growth can arise from the loss of semivolatiles by photolysis, further reaction with OH to form volatile products, or irreversible loss to chamber walls. Such processes reduce the amount of gas-phase semivolatiles that partition into the aerosol phase. The effect on SOA growth of gas-phase reaction forming more volatile species has been examined in a recent modeling study (Chan et al., 2007). Figure 12 shows a kinetic scheme depicting the competition between gas-particle partitioning and irreversible loss of the gas-phase semivolatiles. X represents the product of generic loss of semivolatile species  $A_g$ ;  $k'_{\text{OH}}$  is the pseudo-first-order rate constant ( $k'_{\text{OH}}=k_{\text{OH}}[\text{OH}]$ ) for reaction of the parent hydrocarbon; and  $k_g$  is the first-order rate constant of loss of semivolatiles. When fitting the observed aerosol growth with this simple kinetic model, it is estimated that  $k_g$  is about 5 times larger than  $k'_{\text{OH}}$ . At the estimated OH concentration of  $\sim 2 \times 10^7 \text{ molecules cm}^{-3}$  under high- $\text{NO}_x$  conditions,  $k'_{\text{OH}}$  for longifolene is  $\sim 9.6 \times 10^{-4} \text{ s}^{-1}$ . A major difference in SOA composition under high- and low- $\text{NO}_x$  conditions is the presence of organic nitrates under high- $\text{NO}_x$  conditions. Thus the loss of organic nitrates (among other gas-phase species) may play a role in the observed deceleration in aerosol growth. The reaction rate constants of small alkyl nitrates with OH are generally of the order of  $10^{-13} \text{ cm}^3 \text{ molecule}^{-1} \text{ s}^{-1}$  (hence pseudo-first-order reaction rate of  $\sim 10^{-6} \text{ s}^{-1}$ ) and their photolysis rates have been measured to be  $\sim 1 \times 10^{-6} \text{ s}^{-1}$  (Talukdar et al., 1997; Finlayson-Pitts and Pitts, 2000). Although the OH reaction rate and photolysis rate of organic nitrates are much slower than the oxidation rate of longifolene, both rates are expected to increase with carbon number (Talukdar et al., 1997; Finlayson-Pitts and Pitts, 2000; Treves and Rudich, 2003). Hence, it is possible that gas-phase reaction of  $\text{C}_{15}$  organic nitrates may be occurring at an appreciable rate. Further study on the OH reaction rate constant and photolysis rate of larger nitrates would be useful in evaluating the importance of gas-phase nitrate chemistry in aerosol formation.

Such a deceleration in SOA growth is not observed in longifolene low- $\text{NO}_x$  experiments. This is in contrast to the rapid decrease in aerosol volume observed in isoprene photooxidation under low- $\text{NO}_x$  conditions, in which photolysis and/or further reactions of organic hydroperoxides may be occurring (Kroll et al., 2006). There is evidence for further reactions with longifolene low- $\text{NO}_x$  SOA as well: the AMS  $m/z$  44 ( $\text{CO}_2^+$ ) mass fraction increases over the course of the experiment (Fig. 9), indicating the SOA is being further oxidized. Unlike with isoprene photooxidation, however, the compounds formed from the further oxidation of longifolene products are likely sufficiently nonvolatile to remain in the particle phase. The photochemistry of larger and more complex hydroperoxides merits further investigation.

### 5.2.2 SOA formation from higher generation products

In Figs. 1 and 3, the growth curves of  $\alpha$ -pinene and longifolene photooxidation exhibit a “hook” at the end of the intermediate  $\text{NO}_x$  experiments, indicating that aerosol growth continues after the complete consumption of the parent hydrocarbon. Organic mass measured by the Q-AMS increases even after all the hydrocarbon is consumed, indicating that this additional aerosol growth is not a result of condensation of inorganic nitrate. Continued aerosol growth can arise from further gas-phase reactions of reactive oxidation products, such as aldehydes and furans, etc, or from further particle-phase reactions. In the intermediate  $\text{NO}_x$  experiments, the NO concentration goes to zero within 20 min after the commencement of photooxidation, owing to the rapid reaction of NO and peroxy radicals ( $\text{HO}_2$  and other peroxy radicals). As a result, a transition from high- $\text{NO}_x$  to low- $\text{NO}_x$  conditions occurs over the course of the experiment, and the final aerosol formed is potentially a mixture of the products formed under both conditions. It is possible that particle-phase reactions, such as the formation of peroxyhemiacetals from hydroperoxides and aldehyde species, may be contributing to the further aerosol growth observed in the intermediate  $\text{NO}_x$  experiments (Johnson et al., 2004, 2005).

## 6 Implications

A series of chamber experiments investigating the  $\text{NO}_x$  dependence of SOA formation from the photooxidation of one monoterpene and two sesquiterpenes is reported here. SOA formation from monoterpenes such as  $\alpha$ -pinene is found to have a similar  $\text{NO}_x$  dependence as isoprene (as well as other hydrocarbons with 10 or fewer carbons, such as aromatic species), in which the aerosol yields are substantially higher under low- $\text{NO}_x$  conditions. The  $\text{NO}_x$  dependence of SOA formation from the two sesquiterpenes is, however, markedly different; for longifolene and aromadendrene, aerosol yields are at their maximum under high- $\text{NO}_x$  conditions. The reason for this reversal of the  $\text{NO}_x$  dependence, while not

unequivocally established here, may be the result of production of highly nonvolatile organic nitrates, the existence of which is suggested by both Q-AMS and filter sample data, and/or isomerization of alkoxy radicals to form low-volatility multifunctional organics.

The increase in SOA yield from photooxidation of the larger biogenic hydrocarbons under high-NO<sub>x</sub> conditions could have implications in terms of the effect of anthropogenically influenced air masses on biogenic SOA formation. In the recent study of de Gouw et al. (2005), it is suggested that over the western Atlantic the majority of the measured organic aerosol is from secondary anthropogenic sources, a conclusion that is somewhat at odds with the radiocarbon measurements that indicate high fractions of “modern” (presumably biogenic) carbon (e.g. Klinedinst and Currie, 1999; Weber et al., 2007). If the production of SOA from biogenic hydrocarbons is enhanced in the presence of NO<sub>x</sub>, observations of enhanced SOA correlated with anthropogenic sources can occur, even for organic carbon of biogenic origin. Large anthropogenic hydrocarbons may exhibit a similar NO<sub>x</sub> behavior as that of the sesquiterpenes studied, as suggested by the substantial SOA yields from the OH-initiated reaction of large alkanes in the presence of ppm levels of NO<sub>x</sub> (Lim and Ziemann, 2005). If the NO<sub>x</sub> behavior observed for longifolene and aromadendrene extends to other sesquiterpenes as well as larger alkanes, the contribution to the total SOA from these compounds in polluted air may actually be higher than previously estimated (Griffin et al., 1999a, b; Carreras-Sospedra et al., 2005; de Gouw et al., 2005).

In this study, we have investigated the NO<sub>x</sub> dependence of SOA formation from photooxidation of only the monoterpene  $\alpha$ -pinene and two sesquiterpenes, each containing one double bond. SOA formation from compounds with two or more double bonds can exhibit characteristics that suggest significant contributions from multiple generation products (Ng et al., 2006) and this may have impacts on the NO<sub>x</sub> dependence. It is clear that the effect of NO<sub>x</sub> on SOA yields from the complete suite of atmospherically relevant aerosol-forming hydrocarbons should be evaluated thoroughly.

## Appendix A

### Description of PTR-MS technique

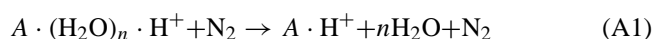
For PTR-MS sampling, a constant flow of  $\sim 2.5$  standard liters per minute (slm) is drawn from the chamber through PFA tubing. The residence time in the inlet tubing is roughly 1 s. A small portion of the flow, 93 standard cubic centimeters per minute (scm), is pulled through a glass critical orifice into a 2.54-cm diameter glass flow tube, in which this sample flow is diluted with dry N<sub>2</sub> (1.6 slm) to maintain the flow tube pressure at 35 mbar. This dilution minimizes confounding effects owing to large concentrations of hydrogen

peroxide and other compounds typically used or produced in chamber experiments.

In the flow tube, analyte ionization occurs in a manner similar to that described by Crouse et al. (2006) for negative ionization. N<sub>2</sub> (400 sccm) flows through an ion source cup composed of a cylindrical silver foil lined with <sup>210</sup>Po and sealed with gold.  $\alpha$  bombardment from the <sup>210</sup>Po, coupled with trace water present in the N<sub>2</sub>, leads to the formation of positively charged clusters, e.g. (H<sub>2</sub>O)<sub>n</sub>H<sup>+</sup>. The electric potentials of the ion source components are set such that these positively charged clusters then pass through a 6.35 mm aperture into the 35 mbar flow tube, flowing perpendicular to the sample flow. The clusters then react via proton transfer with the analyte (e.g. aromadendrene) in the sample flow to form aromadendrene-H<sup>+</sup> and higher order water clusters.

Across the flow tube from the ion source, a pinhole aperture (diameter 0.34 mm) allows a portion of the ions and neutral gas ( $\sim 30$  sccm) to flow into the mass spectrometer, a Varian 1200 tandem mass spectrometer. The spectrometer was modified by removing the electron impact source and extending the hexapole ion guide that leads to the quadrupole mass analyzer to the pinhole aperture. For these measurements, the mass spectrometer was operated exclusively in one-dimensional mass spectrometry mode.

In order to simplify the mass spectra, a DC potential of  $-10$  V (relative to the pinhole aperture) is applied to the hexapole. This offset pulls ions into the hexapole, where the pressure is relatively high owing to the neutral gas flow (chiefly N<sub>2</sub>) through the pinhole. The ions therefore undergo high energy collisions with the neutral gas molecules which dissociate water clusters of analyte A:



Thus, species are predominantly observed at  $m/z = M+1$ , where M is the molecular mass of the species. Hydrates, A·(H<sub>2</sub>O)<sub>m</sub>·H<sup>+</sup>, particularly  $m=1$ , are also observed for some species, though not for aromadendrene or longifolene.

Each day, the PTR-MS sensitivity towards aromadendrene was determined by sampling standard mixtures of aromadendrene in teflon bags filled with 50 L zero air. The sensitivity was determined to be linear from 0 ppb to at least 5 ppb. Also, because of the large amounts of H<sub>2</sub>O<sub>2</sub> utilized in the experiments, the sensitivity as a function of H<sub>2</sub>O<sub>2</sub> was determined, with [H<sub>2</sub>O<sub>2</sub>] measured by operating the Varian 1200 in negative ionization mode, exploiting the reaction of CF<sub>3</sub>O<sup>-</sup> with H<sub>2</sub>O<sub>2</sub> (Crouse et al., 2006). Thus, the sensitivity determined from H<sub>2</sub>O<sub>2</sub>-free standards was corrected for sampling from the chamber when H<sub>2</sub>O<sub>2</sub> was present.

The uncertainty of aromadendrene measurements using PTR-MS is estimated to be  $\sim \pm 22\%$ , based on the scatter of replicate data and background measurements and uncertainties in the H<sub>2</sub>O<sub>2</sub> correction.

## Appendix B

### Description of UPLC/ESI-TOFMS technique

Filter extracts (in 1:1 (v/v) solvent mixture of methanol and 0.1% aqueous acetic acid solution) are analyzed by a Waters ACQUITY ultra performance liquid chromatography (UPLC) system, coupled with a Waters LCT Premier time-of-flight (TOF) mass spectrometer (MS) equipped with an electrospray ionization (ESI) source. The ESI source on this instrument contains two individual sprays; one spray is for the eluent and the other is for the lock-mass correction. Optimum ESI conditions are found using a 2.5 kV capillary voltage, 40 V sample cone voltage, 350°C desolvation temperature, 130°C source temperature, 20 L h<sup>-1</sup> cone gas flow rate, and a 650 L h<sup>-1</sup> desolvation gas flow rate. Data are collected from *m/z* 50–1000 in the negative (–) ionization mode using the TOFMS operated in the W geometry reflectron mode. The W reflectron mode offers the highest mass resolution, which is approximately 12 000, and allows for exact mass measurements to be conducted on detected SOA components. The chromatographic separations are carried out on a Waters ACQUITY HPLC HSS (high strength silica) column (2.1 × 100 mm, 1.8 μm particle size) at 45°C using a gradient elution scheme. The eluent composition is (A) 0.1% acetic acid in water and (B) 0.1% acetic acid in methanol; both eluents are high purity solvents (LC-MS ChromaSolv Grade, Sigma-Aldrich). In the 12-min gradient elution program used, the concentration of eluent B is 0% for the first 2 min, increased to 90% from 2 to 10 min, held at 90% from 10 to 10.2 min; and then decreased back to 0% from 10.2 to 12 min. The flow rate of the eluent is 0.3 mL min<sup>-1</sup> and the sample injection volume is 2 μL. At the beginning of each analysis period, the TOFMS is calibrated using a 1:1 (v/v) solvent mixture of acetonitrile and 0.1% phosphoric acid aqueous solution. During each chromatographic run, 2 ng/μL of leucine enkephalin (MW=555) is used for the lock-mass spray for lock-mass correction to obtain accurate masses for each SOA component eluting from the column. The lock-mass syringe pump is operated at 20 μL min<sup>-1</sup>. In addition to the lock-mass spray, the dynamic range enhancement feature of this mass spectrometer is applied to prevent dead time, which affects mass accuracy, from occurring. As confirmation of the UPLC/ESI-TOFMS technique, a standard sample containing known isoprene and α-pinene sulfate esters previously characterized by Surratt et al. (2007) are analyzed. The known elemental compositions (i.e. molecular formulas) of the previously characterized sulfate esters (Surratt et al., 2007) are in excellent agreement with their measured exact masses (i.e. within ±2 mDa or ±2 ppm). In addition to exact mass measurements, further insights into the structures of the SOA components are obtained by generating tandem MS data, which are generated by increasing the first aperture voltage on the TOFMS from 10 V to 25 V.

**Acknowledgements.** This research was funded by U.S. Department of Energy Biological and Environmental Research Program grant DE-FG02-05ER63983. This material is based in part on work supported by the National Science Foundation (NSF) under grant ATM-0432377. The Waters LCT Premier XT time-of-flight mass spectrometer interfaced to a Waters UPLC system was purchased in 2006 with a grant from the National Science Foundation, Chemistry Research Instrumentation and Facilities Program (CHE-0541745). The LCQ Ion Trap mass spectrometer was purchased in 1997 with funds from the National Science Foundation through the CRIF program (CHE-9709233). J. D. Surratt is supported in part by the U.S. EPA under the STAR Graduate Fellowship Program. A. J. Kwan acknowledges the support of a NSF graduate research fellowship. The authors would like to thank M. Shahgohli of the Chemistry Department at Caltech for her useful communications regarding high-resolution mass spectrometry.

Edited by: A. Nenes

### References

- Alfarra, M. R., Paulsen, D., Gysel, M., Garforth, A. A., Dommen, J., Prevot, A. S. H., Worsnop, D. R., Baltensperger, U., and Coe, H.: A mass spectrometric study of secondary organic aerosols formed from the photooxidation of anthropogenic and biogenic precursors in a reaction chamber, *Atmos. Chem. Phys.*, 6, 5279–5293, 2006, <http://www.atmos-chem-phys.net/6/5279/2006/>.
- Arey, J., Aschmann, S. M., Kwok, E. S. C., and Atkinson, R.: Alkyl nitrates, hydroxyalkyl nitrates and hydroxycarbonyl formation from the NO<sub>x</sub> – air photooxidation of C<sub>5</sub>–C<sub>8</sub> n-alkanes, *J. Phys. Chem. A*, 105, 1020–1027, 2001.
- Aschmann, S. M., Arey, J., and Atkinson, R.: Atmospheric chemistry of three C<sub>10</sub> alkanes, *J. Phys. Chem. A*, 105, 7598–7606, 2001.
- Aschmann, S. M., Atkinson, R., and Arey, J.: Products of reaction of OH radicals with α-pinene, *J. Geophys. Res.*, 107(D14), 4191, doi:10.1029/2001JD001098, 2002.
- Aschmann, S. M., Reissell, A., Atkinson, R., and Arey, J.: Products of the gas phase reactions of the OH radical with α- and β-pinene in the presence of NO, *J. Geophys. Res.*, 103(D19), 4191, 25 553–25 561, 1998.
- Aschmann, S. M., Reissell, A., Atkinson, R., and Arey, J.: Products of the gas phase reactions of the OH radical with α- and β-pinene in the presence of NO, *J. Geophys. Res.*, 103(D19), 25 553–25 561, 1998.
- Atkinson, R., Kwok, E. S. C., Arey, J., and Aschmann, S. M.: Reactions of alkoxy radicals in the atmosphere, *Faraday Discuss.*, 100, 23–37, 1995.
- Atkinson, R. and Arey, J.: Gas-phase tropospheric chemistry of biogenic volatile organic compounds: a review, *Atmos. Environ.*, 37, S197–S219, 2003.
- Atkinson, R., Aschmann, S. M., and Winer, A. M.: Alkyl nitrate formation from the reaction of a series of branched RO<sub>2</sub> radicals with NO as a function of temperature and pressure, *J. Phys. Chem.*, 5, 91–102, 1987.
- Atkinson, R., Baulch, D. L., Cox, R. A., Hampson, R. F., Kerr, J. A., Rossi, M. J., and Troe, J.: Evaluated kinetic and photochemical



- data for atmospheric chemistry, organic species, supplement VII, *J. Phys. Chem. Ref. Data.*, 28, 2, 1999.
- Atkinson, R.: Atmospheric reactions of alkoxy and  $\beta$ -hydroxyalkoxy radicals, *Int. J. Chem. Kinet.*, 29, 99–111, 1997a.
- Atkinson, R.: Gas phase tropospheric chemistry of organic compounds, *J. Phys. Chem. Ref. Data, Monogr.*, 2, 11–216, 1994.
- Atkinson, R.: Gas phase tropospheric chemistry of volatile organic compounds: 1. Alkanes and Alkenes, *J. Phys. Chem. Ref. Data.*, 215–290, 1997b.
- Baldwin, A. C., Barker, J. R., Golden, D. M., and Hendry, D. G.: Photochemical smog – rate parameter estimates and computer simulations, *J. Phys. Chem.*, 81, 2483–2492, 1977.
- Bahreini, R., Keywood, M. D., Ng, N. L., Varutbangkul, V., Gao, S., Flagan, R. C., and Seinfeld, J. H.: Measurements of secondary organic aerosol (SOA) from oxidation of cycloalkenes, terpenes, and m-xylene using an Aerodyne aerosol mass spectrometer, *Environ. Sci. Technol.*, 39, 5674–5688, 2005.
- Carreras-Sospedra, M., Griffin, R. J., and Dabdub, D.: Calculations of incremental secondary organic aerosol reactivity, *Environ. Sci. Technol.*, 39, 1724–1730, 2005.
- Carter, W. P. L. and Atkinson, R.: Alkyl nitrate formation from the atmospheric photooxidation of alkanes; a revised estimation, *J. Phys. Chem.*, 8, 165–173, 1989.
- Carter, W. P. L. and Atkinson, R.: Atmospheric chemistry of alkanes, *J. Atmos. Chem.* 3, 377–405, 1985.
- Chan, A. W. H., Kroll, J. H., Ng, N. L., and Seinfeld, J. H.: Kinetic modeling of secondary organic aerosol formation: effect of particle- and gas-phase reactions of semivolatile products, *Atmos. Chem. Phys. Discuss.*, 7, 7051–7085, 2007, <http://www.atmos-chem-phys-discuss.net/7/7051/2007/>.
- Cocker III, D. R., Flagan, R. C., and Seinfeld, J. H.: State-of-the-art chamber facility for studying atmospheric aerosol chemistry, *Environ. Sci. Technol.*, 35, 2594–2601, 2001.
- Crounse, J. D., McKinney, K. A., Kwan, A. J., and Wennberg, P. O.: Measurements of gas-phase hydroperoxides by chemical ionization mass spectrometry, *Anal. Chem.*, 78, 6726–6732, 2006.
- de Gouw, J. A., Middlebrook, A. M., Warneke, C., Goldan, P. D., Kuster, W. C., Roberts, J. M., Fehsenfeld, F. C., Worsnop, D. R., Canagaratna, M. R., Pszenny, A. A. P., Keene, W. C., Marchewka, M., Bertman, S. B., and Bates, T. S.: Budget of organic carbon in a polluted atmosphere: Results from the New England Air Quality Study in 2002, *J. Geophys. Res.*, 110, D16305, doi:10.1029/2004JD005623, 2005.
- Finlayson-Pitts, B. J. and Pitts, J. N.: Chemistry of the upper and lower atmosphere: theory, experiments and applications, Academic Press, San Diego, 220–221, 2000.
- Gao, S., Keywood, M. D., Ng, N. L., Surratt, J. D., Varutbangkul, V., Bahreini, R., Flagan, R. C., and Seinfeld, J. H.: Low-molecular weight and oligomeric components in secondary organic aerosol from the ozonolysis of cycloalkenes and  $\alpha$ -pinene, *J. Phys. Chem. A*, 108, 10 147–10 164, 2004.
- Gao, S., Surratt, J. D., Knipping, E. M., Edgerton, E. S., Shahgholi, M., and Seinfeld, J. H.: Characterization of polar organic components in fine aerosols in the southeastern United States: Identity, origin, and evolution, *J. Geophys. Res.*, 111, D14314, doi:10.1029/2005JD006601, 2006.
- Geron, C., Rasmussen, R., Arnts, R. R., and Guenther, A.: A review and synthesis of monoterpene speciation from forests in the United States, *Atmos. Environ.*, 34, 1761–1781, 2000.
- Glasius, M., Duane, M., and Larsen, B. R.: Determination of polar terpene oxidation products in aerosols by liquid chromatography-ion trap mass spectrometry, *J. Chrom. A.*, 833, 121–135, 1999.
- Glasius, M., Lahaniati, M., Calogirou, A., Di Bella, D., Jensen, N. R., Hjorth, J., Kotzias, D., and Larsen, B. R.: Carboxylic acids in secondary aerosols from oxidation of cyclic monoterpenes by ozone, *Environ. Sci. Technol.*, 34, 1001–1010, 2000.
- Griffin, R. J., Cocker, D. R., Flagan, R. C., Seinfeld, J. H., and Dabdub, D.: Estimate of global atmospheric organic aerosol formation from the oxidation of biogenic hydrocarbons, *Geophys. Res. Lett.*, 26, 17, 2721–2724, 1999a.
- Griffin, R. J., Cocker, D. R., Flagan, R. C., and Seinfeld, J. H.: Organic aerosol formation from the oxidation of biogenic hydrocarbons, *J. Geophys. Res.*, 104(D3), 3555–3567, 1999b.
- Guenther, A., Hewitt, C. N., Erickson, D., Fall, R., Geron, C., Graedel, T., Harley, P., Klinger, L., Lerdau, M., McKay, W. A., Pierce, T., Scholes, B., Steinbrecher, R., Tallamraju, R., Taylor, T., and Zimmerman, P.: A global model of natural volatile organic compound emission, *J. Geophys. Res.*, 100, (D5), 8873–8892, 1995.
- Hatakeyama, S., Izumi, K., Fukuyama, T., Akimoto, H., and Washida, N.: Reactions of OH with  $\alpha$ -pinene and  $\beta$ -pinene in air: Estimates of global CO production from the atmospheric oxidation of terpenes, *J. Geophys. Res.*, 96(D1), 947–958, 1991.
- Hurley, M. D., Sokolov, O., Wallington, T. J., Takekawa, H., Karasawa, M., Klotz, B., Barnes, I., and Becker, K. H.: Organic aerosol formation during the atmospheric degradation of toluene, *Environ. Sci. Technol.*, 35, 1358–1366, 2001.
- Jayne, J. T., Leard, D. C., Zhang, X., Davidovits, P., Smith, K. A., Kolb, C. E., and Worsnop, D. W.: Development of an Aerosol Mass Spectrometer for size and composition analysis of submicron particles, *Aerosol Sci. Tech.*, 33, 49–70, 2000.
- Johnson, D., Jenkin, M. E., Wirtz, K., and Martín-Reviejo, M.: Simulating the formation of secondary organic aerosol from the photooxidation of aromatic hydrocarbons, *Environ. Chem.*, 2, 35–48, 2005.
- Johnson, D., Jenkin, M. E., Wirtz, K., and Martín-Reviejo, M.: Simulating the formation of secondary organic aerosol from the photooxidation of toluene, *Environ. Chem.*, 1, 150–165, 2004.
- Kanakidou, M., Seinfeld, J. H., Pandis, S. N., Barnes, I., Dentener, F. J., Facchini, M. C., Van Dingenen, R., Evers, B., Nenes, A., Swietlicki, E., Pautaud, J. P., Balkanski, Y., Fuzzi, S., Horth, J., Moortgat, G. K., Winterhalter, R., Myhre, C. E. L., Tsigaridis, K., Vignati, E., Stephanou, E. G., and Wilson, J.: Organic aerosol and global climate modeling: a review, *Atmos. Chem. Phys.*, 5, 1053–1123, 2005, <http://www.atmos-chem-phys.net/5/1053/2005/>.
- Keywood, M. D., Varutbangkul, V., Bahreini, R., Flagan, R. C., and Seinfeld, J. H.: Secondary organic aerosol formation from the ozonolysis of cycloalkenes and related compounds, *Environ. Sci. Technol.*, 38, 4157–4164, 2004.
- Klinedinst, D. B. and Currie, L. A.: Direct quantification of PM<sub>2.5</sub> fossil and biomass carbon within the northern front range air quality study's domain, *Environ. Sci. Technol.*, 33, 4146–4154, 1999.
- Kroll, J. H., Ng, N. L., Murphy, S. M., Flagan, R. C., and Seinfeld, J. H.: Secondary organic aerosol formation from isoprene photooxidation under high-NO<sub>x</sub> conditions, *J. Geophys. Res.*, 32,

- L18808, doi:10.1029/2005GL023637, 2005.
- Kroll, J. H., Ng, N. L., Murphy, S. M., Flagan, R. C., and Seinfeld, J. H.: Secondary organic aerosol formation from isoprene photooxidation, *Environ. Sci. Technol.*, 40, 1869–1877, 2006.
- Larsen, B. R., Di Bella, D., Glasius, M., Winterhalter, R., Jensen, N. R., and Hjorth, J.: Gas-phase OH oxidation of monoterpenes: Gaseous and particulate products, *J. Atmos. Chem.*, 38, 231–276, 2001.
- Lim, Y. B. and Ziemann, P. J.: Products and mechanism of secondary organic aerosol formation from reactions of *n*-alkanes with OH radicals in the presence of NO<sub>x</sub>, *Environ. Sci. Technol.*, 39, 9229–9236, 2005.
- Ng, N. L., Kroll, J. H., Keywood, M. D., Bahreini, R., Varutbangkul, V., Flagan, R. C., Seinfeld, J. H., Lee, A., and Goldstein, A. H.: Contribution of first- versus second-generation products to secondary organic aerosols formed in the oxidation of biogenic hydrocarbons, *Environ. Sci. Technol.*, 40, 2283–2297, 2006.
- Ng, N. L., Kroll, J. H., Chan, A. W. H., Chhabra, P. S., Flagan, R. C., and Seinfeld, J. H.: Secondary organic aerosol formation from *m*-xylene, toluene, and benzene, *Atmos. Chem. Phys. Discuss.*, 7, 4085–4126, 2007, <http://www.atmos-chem-phys-discuss.net/7/4085/2007/>.
- O'Brien, J. M., Czuba, E., Hastie, D. R., Francisco, J. S., and Shepson, P. B.: Determination of the hydroxy nitrate yields from the reaction of C<sub>2</sub>–C<sub>6</sub> alkenes with OH in the presence of NO, *J. Phys. Chem.*, 102, 8903–8908, 1998.
- Odum, J. R., Hoffmann, T., Bowman, F., Collins, D., Flagan, R. C., and Seinfeld, J. H.: Gas/particle partitioning and secondary organic aerosol yields, *Environ. Sci. Technol.*, 30, 2580–2585, 1996.
- Odum, J. R., Jungkamp, T. P. W., Griffin, R. J., Forstner, H. J. L., Flagan, R. C., and Seinfeld, J. H.: Aromatics, reformulated gasoline and atmospheric organic aerosol formation, *Environ. Sci. Technol.*, 31, 1890–1897, 1997.
- Owen, S. M., Boissard, C., and Hewitt, C. N.: Volatile organic compounds (VOCs) emitted from 40 Mediterranean plan species: VOC speciation and extrapolation to habitat scale, *Atmos. Environ.*, 35, 5393–5409, 2001.
- Pandis, S. N., Paulson, S. E., Seinfeld, J. H., and Flagan, R. C.: Aerosol formation in the photooxidation of isoprene and  $\beta$ -pinene, *Atmos. Environ.*, 25A, 997–1008, 1991.
- Presto, A. A., Huff Hartz, K. E., and Donahue, N. M.: Secondary organic aerosol production from ozonolysis: 2. Effect of NO<sub>x</sub> concentration, *Environ. Sci. Technol.*, 39, 7046–7054, 2005.
- Seinfeld, J. and Pankow, J. F.: Organic atmospheric particulate material, *Annu. Rev. Phys. Chem.*, 54, 121–140, 2003.
- Song, C., Na, K., and Cocker III, D. R.: Impact of the hydrocarbon to NO<sub>x</sub> ratio on secondary organic aerosol formation, *Environ. Sci. Technol.*, 39, 3143–3149, 2005.
- Sorooshian, A., Brechtel F. J., Ma, Y. L., Weber R. J., Corless, A., Flagan, R. C., and Seinfeld, J. H.: Modeling and characterization of a particle-into-liquid sampler (PILS), *Aerosol Sci. Tech.*, 40, 396–409, 2006.
- Surratt, J. D., Kroll, J. H., Kleindienst, T. E., Edney, E. O., Claeys, M., Sorooshian, A., Ng, N. L., Offenberg, J. H., Lewandowski, M., Jaoui, M., Flagan, R. C., and Seinfeld, J. H.: Evidence for organosulfates in secondary organic aerosol, *Environ. Sci. Technol.*, 41, 517–527, 2007.
- Surratt, J. D., Murphy, S. M., Kroll, J. H., Ng, N. L., Hildebrandt, L., Sorooshian, A., Szmigielski, R., Vermeylen, R., Maenhaut, W., Claeys, M., Flagan, R. C., and Seinfeld, J. H.: Chemical composition of secondary organic aerosol formed from the photooxidation of isoprene, *J. Atmos. Chem.*, 31, 9665–9690, 2006.
- Szmigielski, R., Surratt, J. D., Vermeylen, R., Szmigielska, K., Kroll, J. H., Ng, N. L., Murphy, S. M., Sorooshian, A., Seinfeld, J. H., and Claeys, M.: Characterization of 2-methylglyceric acid oligomers in secondary organic aerosol formed from the photooxidation of isoprene using trimethylsilylation and gas chromatography/ion trap mass spectrometry, *J. Mass Spectrom.*, 42, 101–116, 2007.
- Talukdar, R. K., Herndon, S. C., Burkholder, J. B., Roberts, J. M., and Ravishankara, A. R.: Atmospheric fate of several alkyl nitrates, *J. Chem. Soc., Faraday Trans.*, 93, 2787–2796, 1997.
- Treves, K. and Rudich, Y.: The atmospheric fate of C<sub>3</sub>–C<sub>6</sub> hydroxyalkyl nitrates, *J. Phys. Chem. A*, 107, 7809–7817, 2003.
- Weber, R. J., Sullivan, A., Peltier, R. E., Russell, A., Yan, B., Zheng, M., de Gouw, J., Warneke, C., Brock, C., Holloway, J. S., Atlas, E. L., and Edgerton, E.: A study of secondary organic aerosol formation in the anthropogenic-influenced southeastern USA, *J. Geophys. Res.*, 112, D13302, doi:10.1029/2007JD008408, 2007.
- Zhang, J., Dransfield, T., and Donahue, N. M.: On the mechanism for nitrate formation via the peroxy radical + NO reaction, *J. Phys. Chem. A*, 108, 9082–9095, 2004.
- Zhang, J., Hartz, K. E. H., Pandis, S. N., and Dohanue, N. M.: Secondary organic aerosol formation from limonene ozonolysis: Homogeneous and heterogeneous influences as a function of NO<sub>x</sub>, *J. Phys. Chem., A*, 110, 11 053–11 063, 2006.
- Zhang, S. H., Shaw, M., Seinfeld, J. H., and Flagan, R. C.: Photochemical aerosol formation from  $\alpha$ -pinene and  $\beta$ -pinene, *J. Geophys. Res.*, 97(D18), 20 717–20 729, 1992.